This paper describes objective technical results and analysis. Any subjective views or opinions that might be expressed in the paper do not necessarily represent the views of the U.S. Department of Energy or the United States Government.

SAND2022-13842C

Sandia National Laboratories

Regional Mechanical Performance and the Effects of Surface Defects in AM Al-10Si-Mg

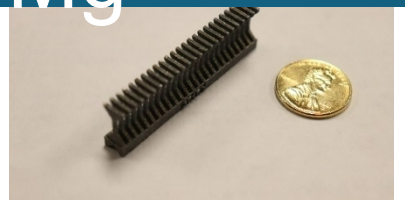

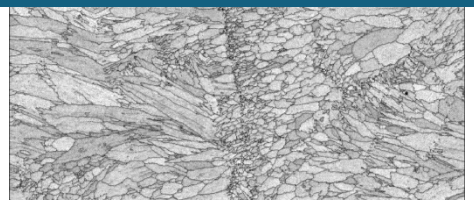

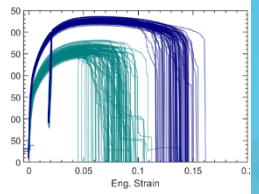

Thomas A. Ivanoff, Nathan M. Heckman, Andrew T. Polonsky, and Kyle L. Johnson

MS&T 2022 Technical Meeting & Exhibition (MS&T 2022)
Pittsburgh, PA
October 10th, 2022

Sandia National Laboratories is a multimission laboratory managed and operated by National Technology & Engineering Solutions of Sandia, LLC, a wholly owned subsidiary of Honeywell International Inc., for the U.S. Department of Energy's National Nuclear Security Administration under contract DE-NA0003525.

Sandia National Laboratories is a multimission laboratory managed and operated by National Technology & Engineering Solutions of Sandia, LLC, a wholly owned subsidiary of Honeywell International Inc., for the U.S. Department of Energy's National Nuclear Security Administration under contract DE-NA0003525.

SAND

Previous work demonstrates variable performance for AM parts caused by internal porosity and spatial variations in structure with differing local responses

1. Previous work demonstrated variability in AM performance

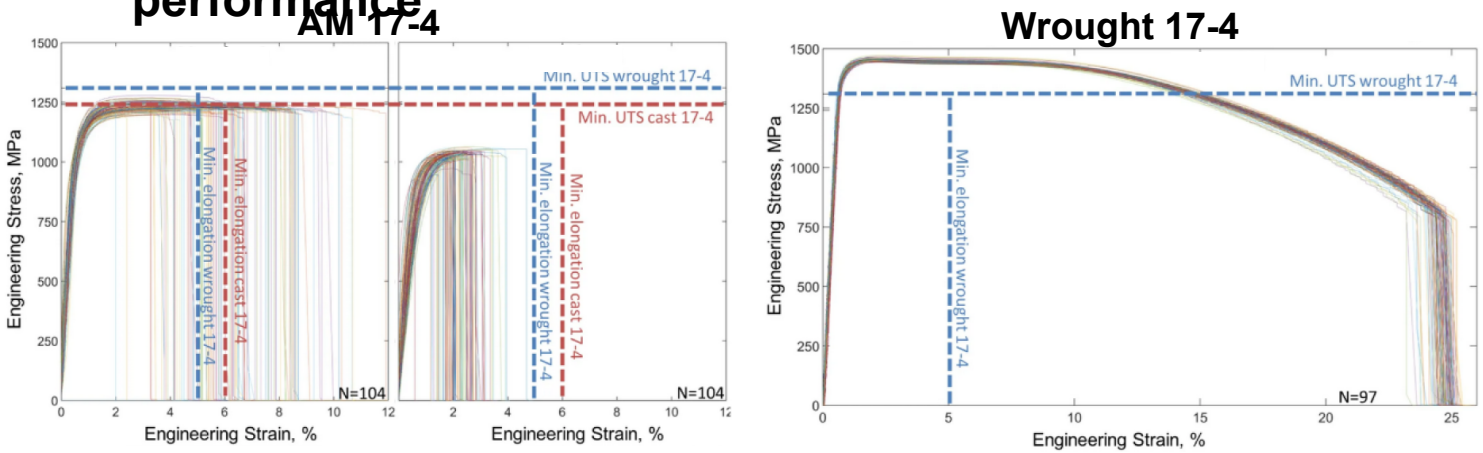

Salzbrenner, B.C, et al. J. Mat. Proc. Tech., 2017

2. Edge effects lead to stochasticity

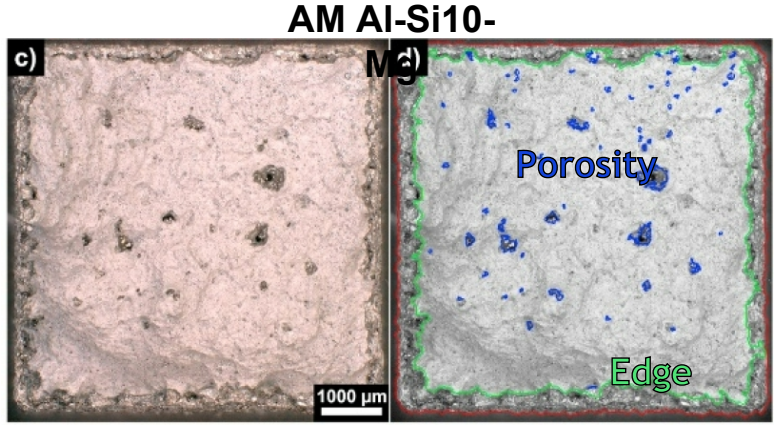

Laursen, C.M. et al. Mat. Sci. Eng. A, 2020

Previous work demonstrates variable performance for AM parts caused by internal porosity and spatial variations in structure with differing local responses

1. Previous work demonstrated variability in AM performance

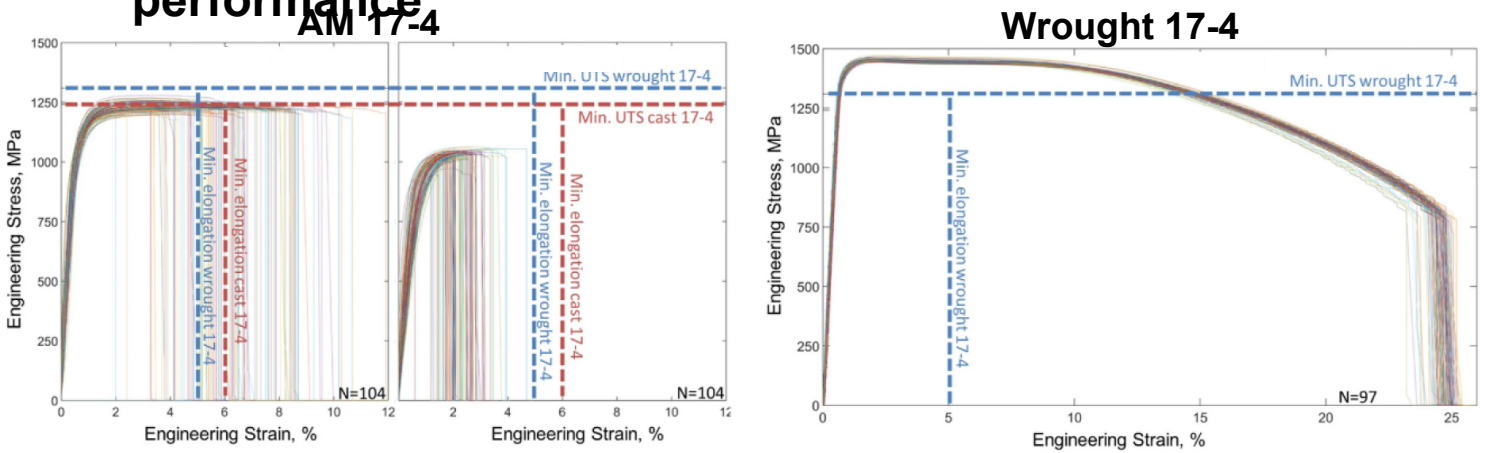

Salzbrenner, B.C, et al. J. Mat. Proc. Tech., 2017

2. Edge effects lead to stochasticity

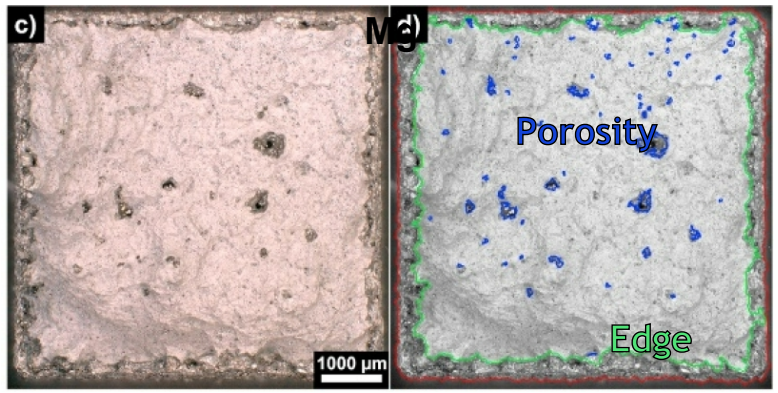

Laursen, C.M. et al. Mat. Sci. Eng. A, 2020

1. **Characterize local behavior in AM metals**

2. **Develop experimentally-informed modeling/meshing solutions to aid AM metals design and qualification**

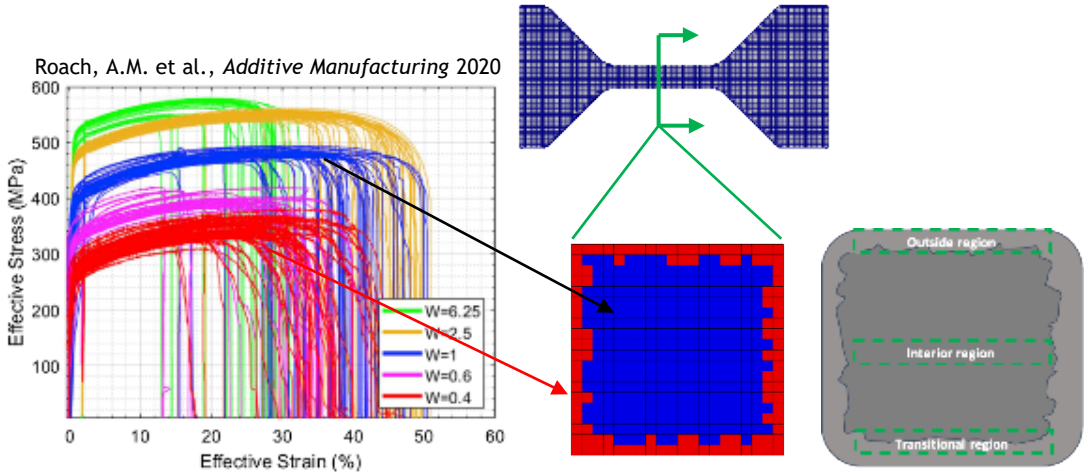

Recent work seeks to develop process-structure-property relationships to enable predictions of mechanical response that aid development/qualification workflows

Current Status

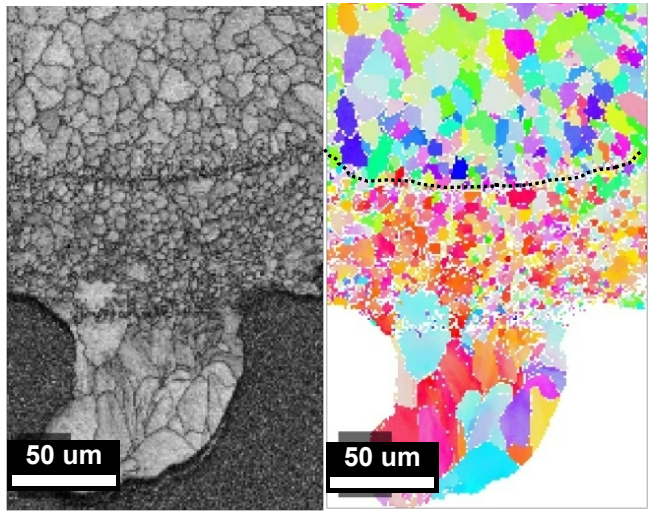

Short Term

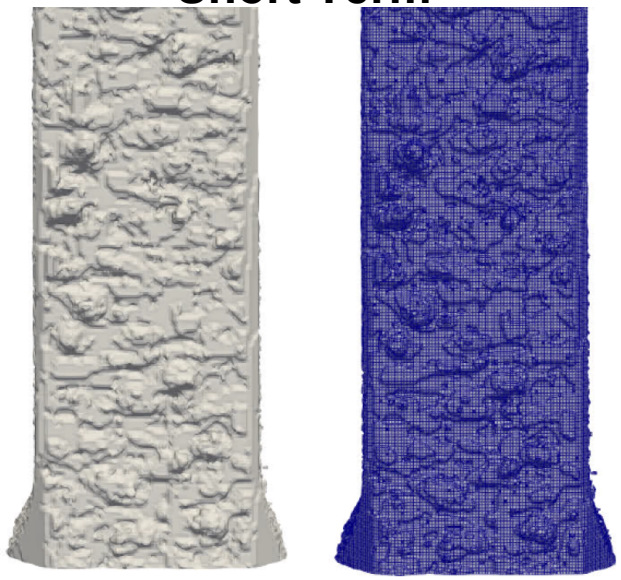

Long Term

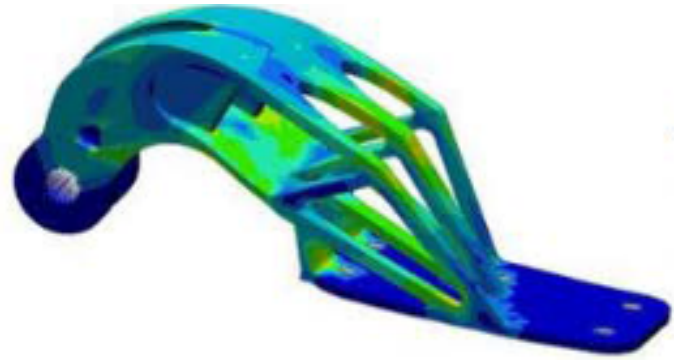

Gebsia, A.W. et al. IOP Conf. Ser: Mater. Sci. Eng., 2017

- Identify dominating edge/local mechanics in AM metals
- Identify distinguishing features of different regions in AM metals

- Incorporate mechanics into high fidelity models
- Validate response in complex geometries

- Reduced fidelity modeling
- First-pass mod/sim technology
- Quantify uncertainty

Recent work seeks to develop process-structure-property relationships to enable predictions of mechanical response that aid development/qualification workflows

Current Status

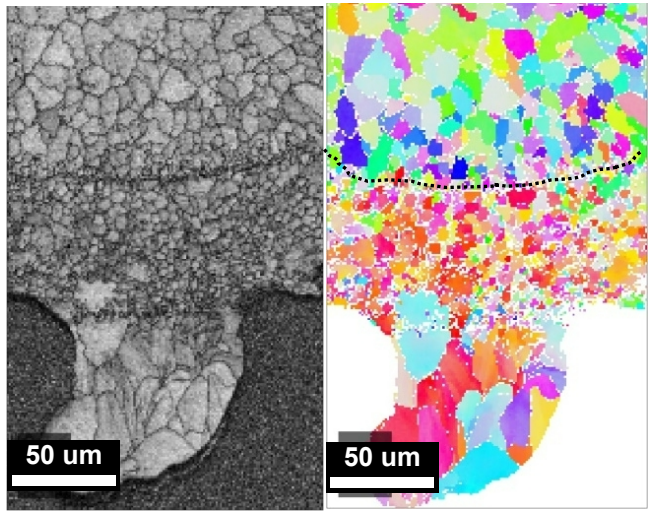

- Identify dominating edge/local mechanics in AM metals
- Identify distinguishing features of different regions in AM metals

Short Term

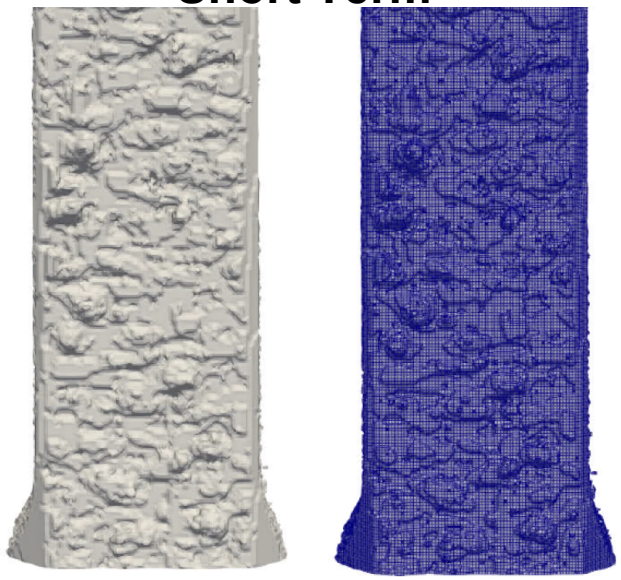

- Incorporate mechanics into high fidelity models
- Validate response in complex geometries

Long Term

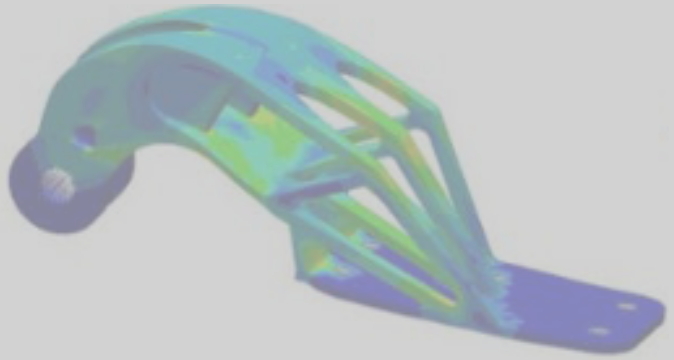

Gebsia, A.W. et al. IOP Conf. Ser: Mater. Sci. Eng., 2017

- Reduced fidelity modeling
- First-pass mod/sim technology
- Quantify uncertainty

Aluminum alloy Al-Si10-Mg produced from LPBF by two vendors. Different tools used but nominally equivalent powder and all material evaluated using sub-sized tensile specimens

Test specimens are sub-sized tensile specimens with a nominal gage area for 1mm x 1mm and a gage length of ~4mm

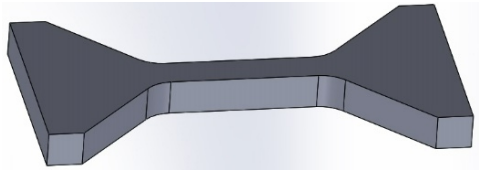

Vendor 1

- Two build geometries investigated from a single build plate:
  - Small build - as-built sub-sized tensile bars
  - Large build - specimens wire EDM from a block of material

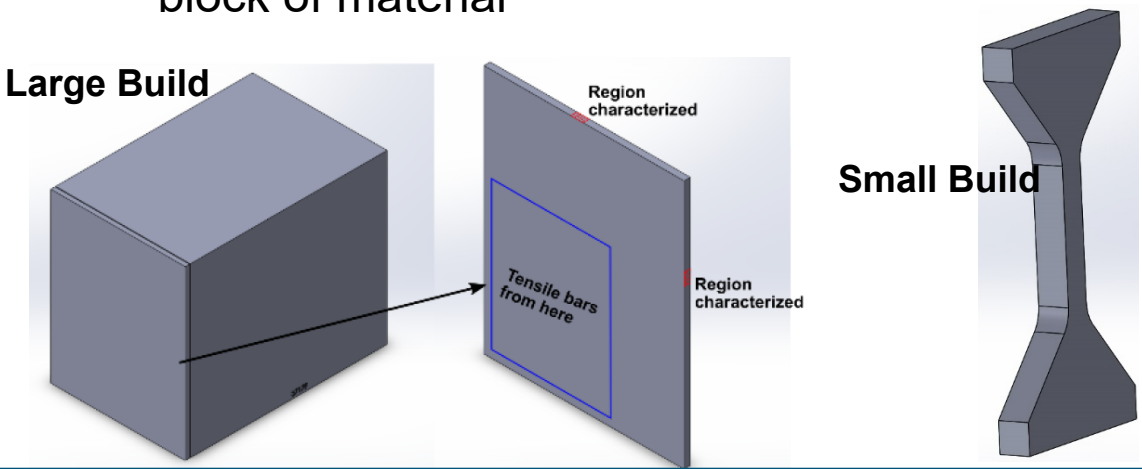

Vendor 2

- Two build geometries investigated from a single build plate:
  - As-built sub-sized tensile bars
  - Large build - specimens wire EDM from a block of material

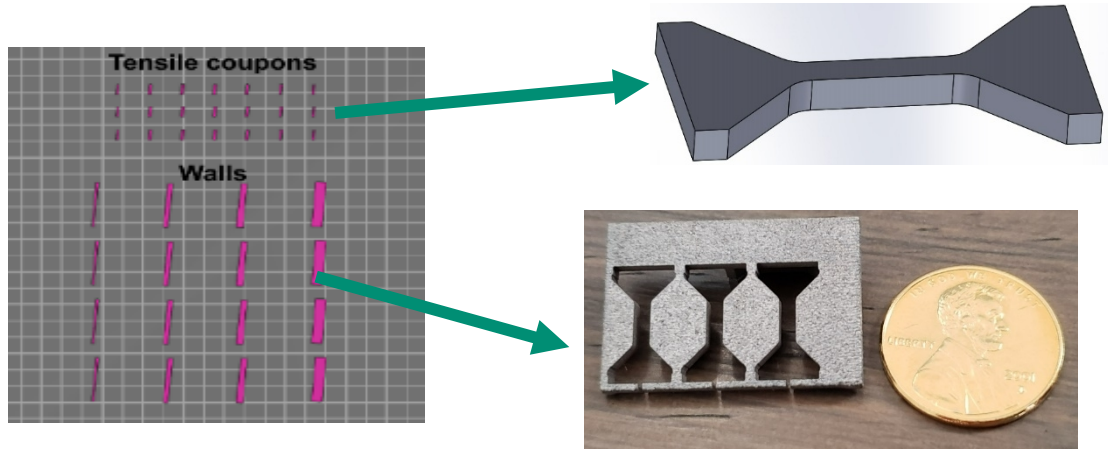

Experimental Methods

Characterization

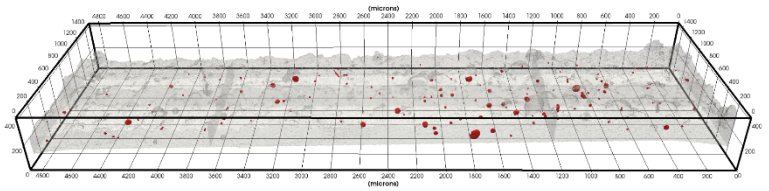

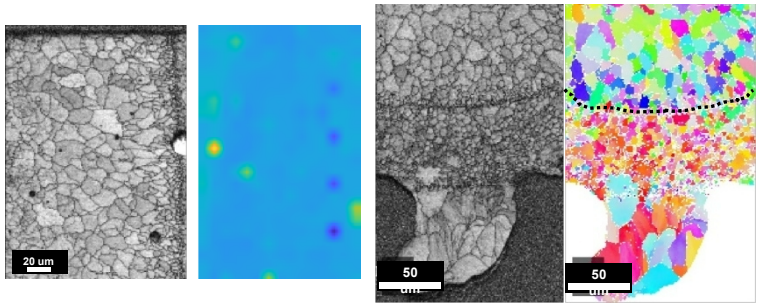

- Identify microstructural features that impact local response (e.g. grain structure and porosity)

- Electron microscopy, micro-computed tomography, nano-indentation

Experimental Methods

Characterization

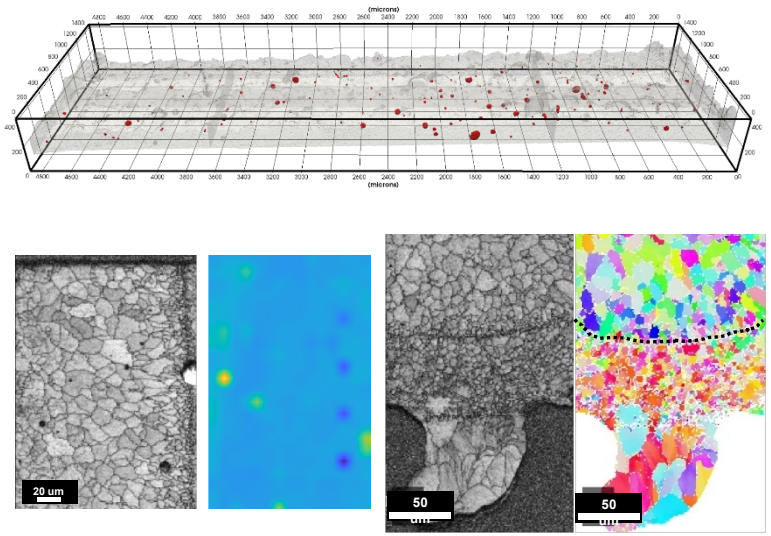

- Identify microstructural features that impact local response (e.g. grain structure and porosity)
- Electron microscopy, micro-computed tomography, nano-indentation

Mechanical Testing

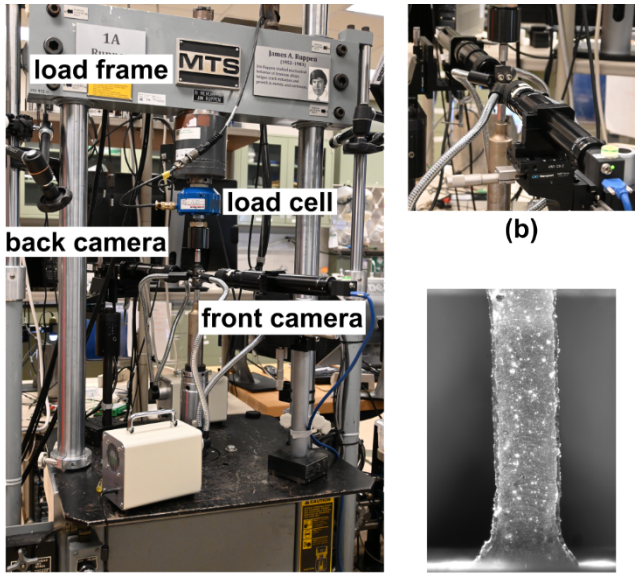

- Determine strength/ductility discrepancies between the surface and interior
- In-situ DIC and micro-computed tomography tensile testing

Experimental Methods

Characterization

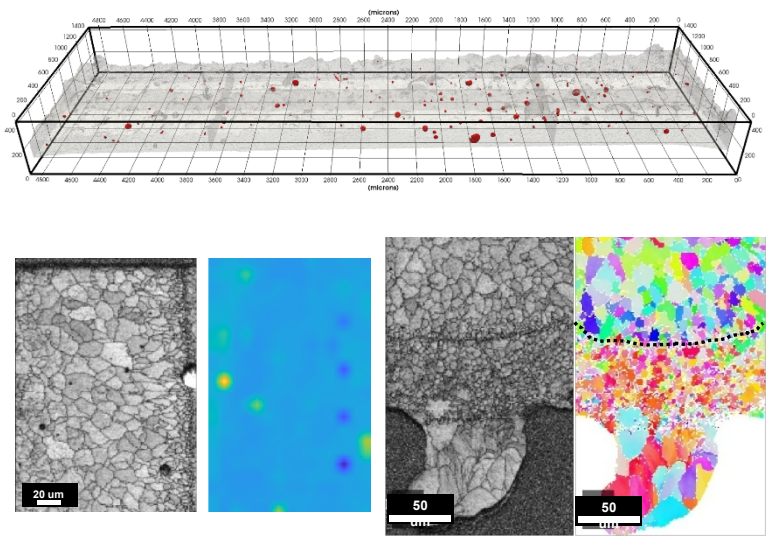

- Identify microstructural features that impact local response (e.g. grain structure and porosity)
- Electron microscopy, micro-computed tomography, nano-indentation

Mechanical Testing

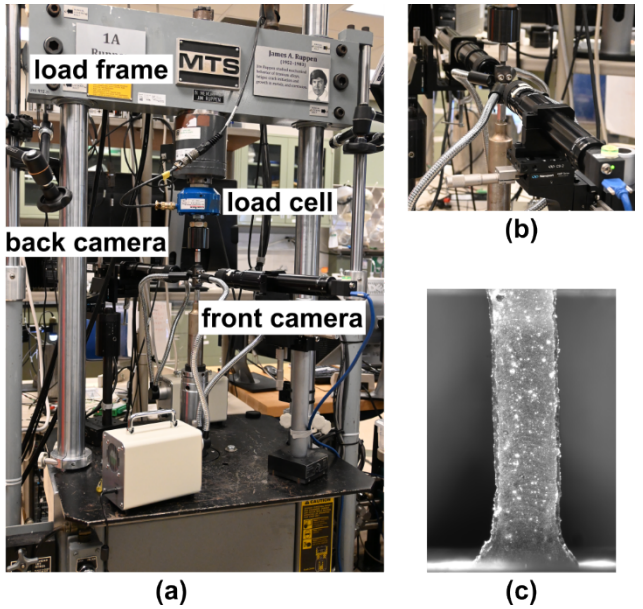

- Determine strength/ductility discrepancies between the surface and interior
- In-situ DIC and micro-computed tomography tensile testing

High-fidelity modeling

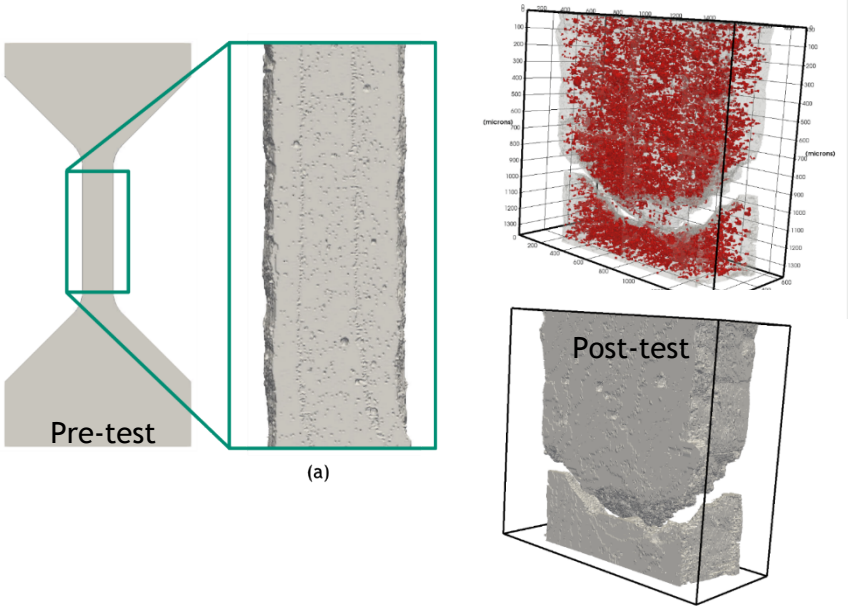

- Determine strength/ductility differences between the surface and interior
- In-situ DIC and micro-computed tomography

Experimental Methods

Characterization

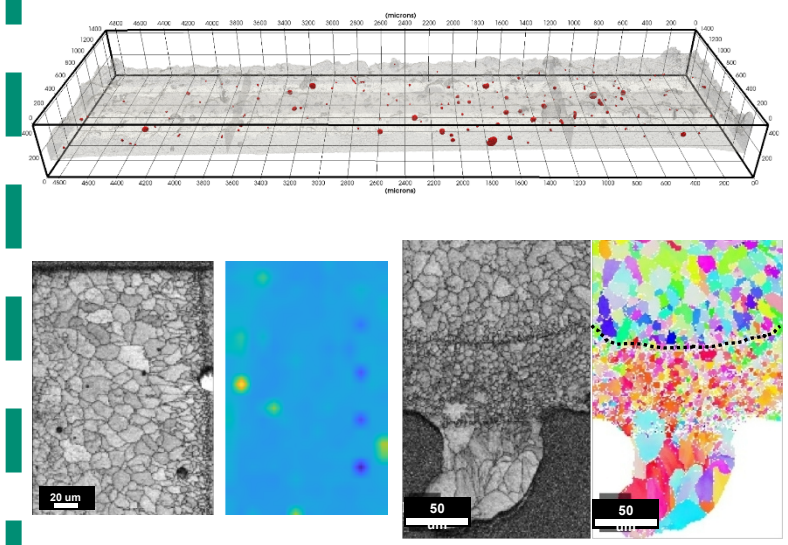

- Identify microstructural features that impact local response (e.g. grain structure and porosity)
- Electron microscopy, micro-computed tomography, nano-indentation

Mechanical Testing

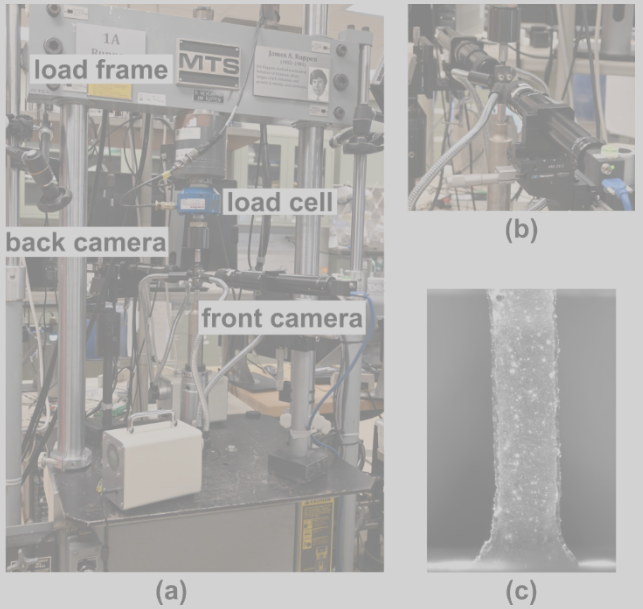

- Determine strength/ductility discrepancies between the surface and interior
- In-situ DIC and micro-computed tomography tensile testing

High-fidelity modeling

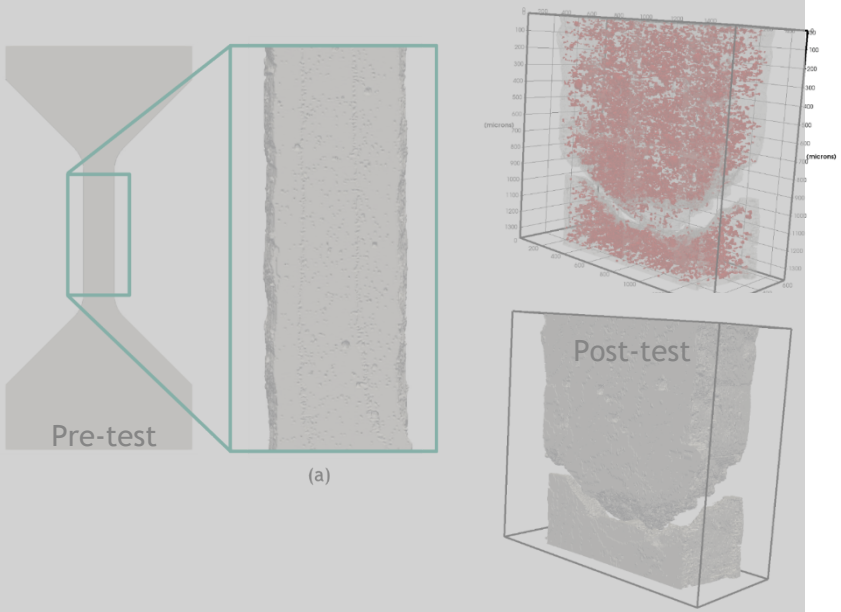

- Determine strength/ductility differences between the surface and interior
- In-situ DIC and micro-computed tomography

Microstructure Vendor 1 – Clear distinction between surface and interior in texture and grain morphology. No strong overall texture but the surface seems to prefer [001] orientation.

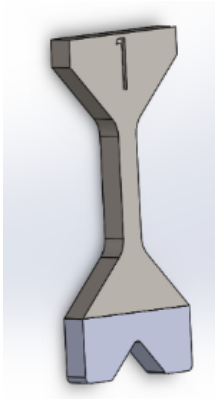

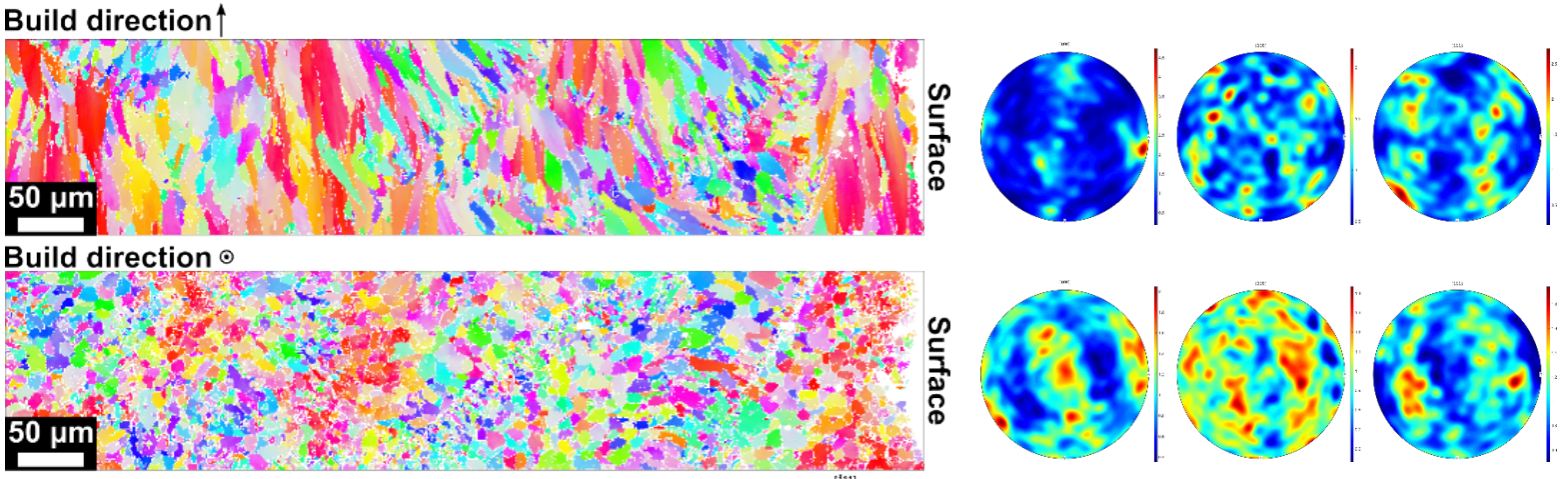

(a) ACQ high-throughput material

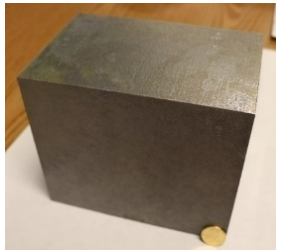

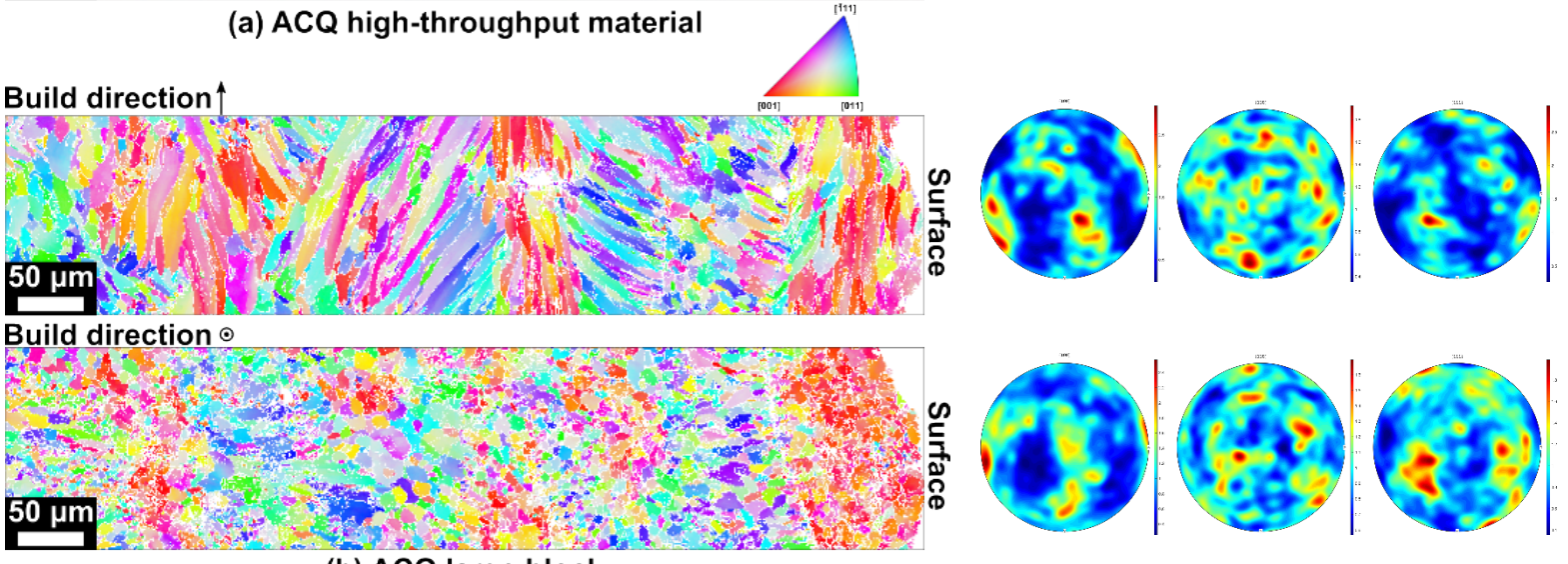

(b) ACQ large block

Microstructure Vendor 2 – Strong distinction between surface and interior in texture and grain morphology. Strong overall texture favors the [001] aligned with the build direction.

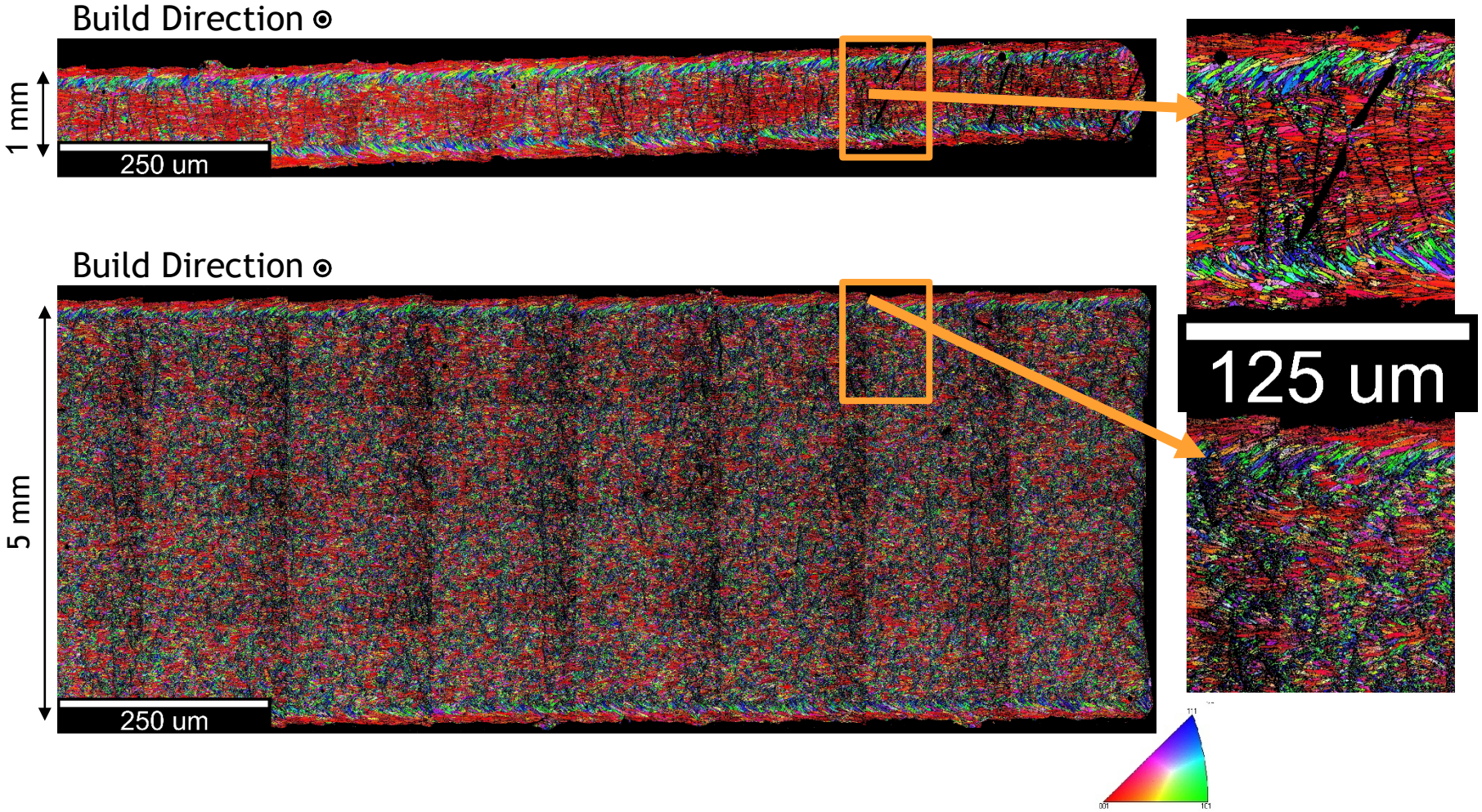

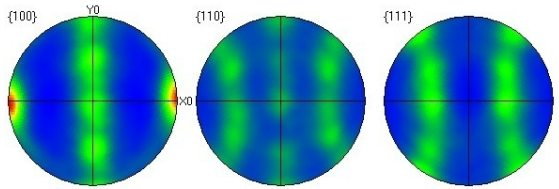

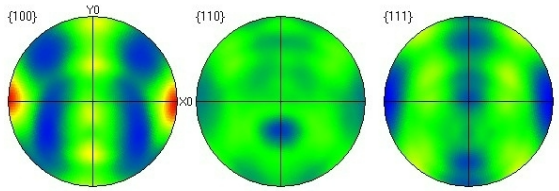

Microstructure Comparison – Variation in grain size and texture along the edge of both materials but stronger in Vendor 2. Higher pore content in Vendor 2 which will impact mechanical response.

Vendor 1

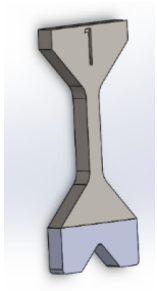

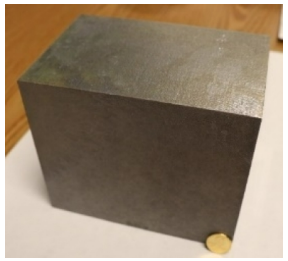

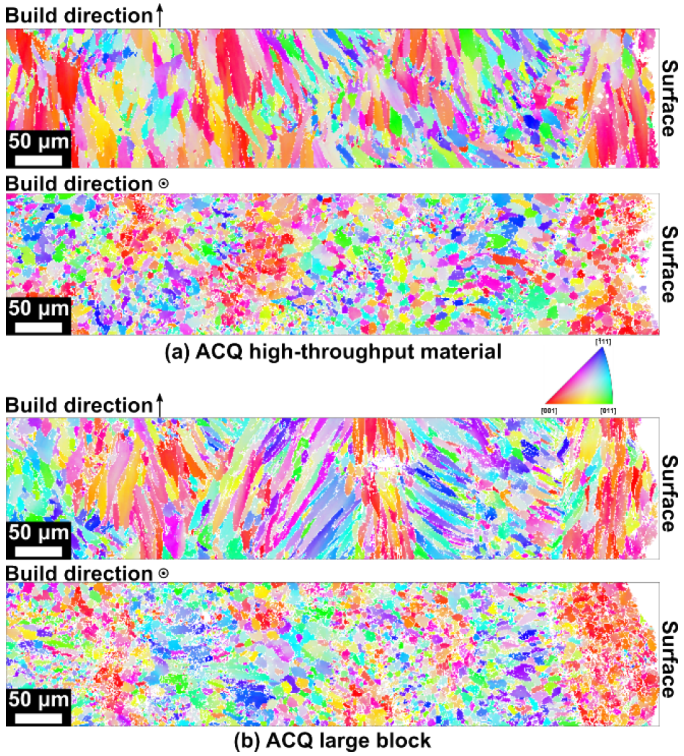

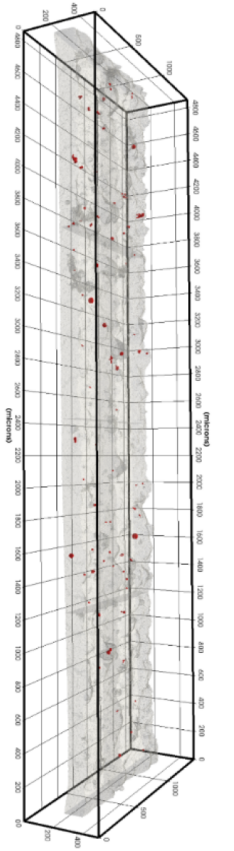

<1% porosity

Vendor 2

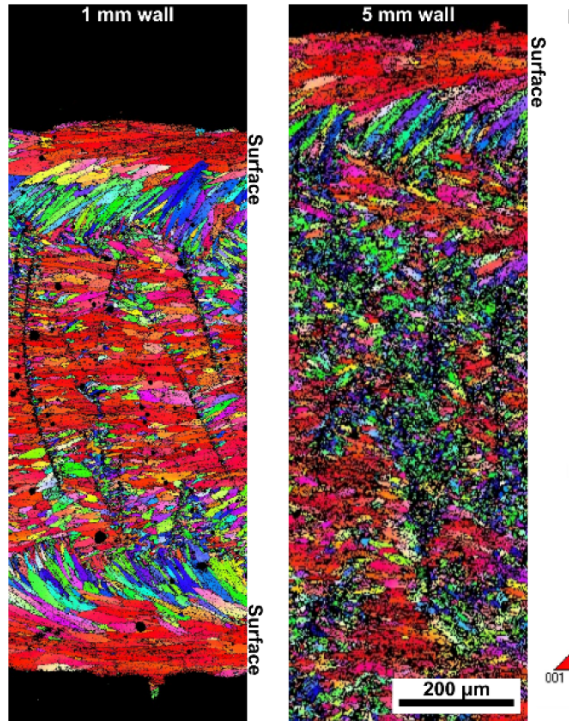

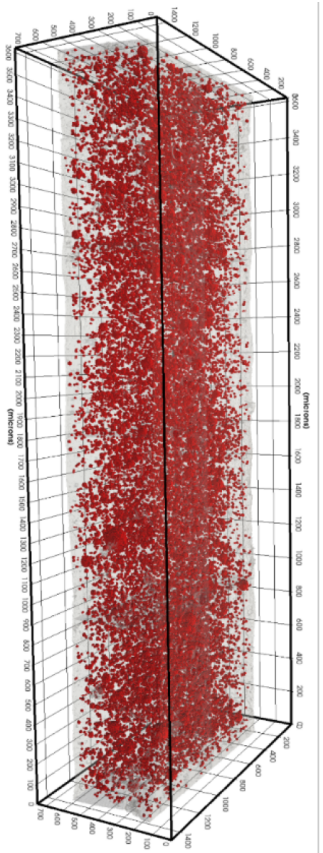

5% porosity

Note: 3D reconstruction can deceptively represent pore content

Experimental Methods

Characterization

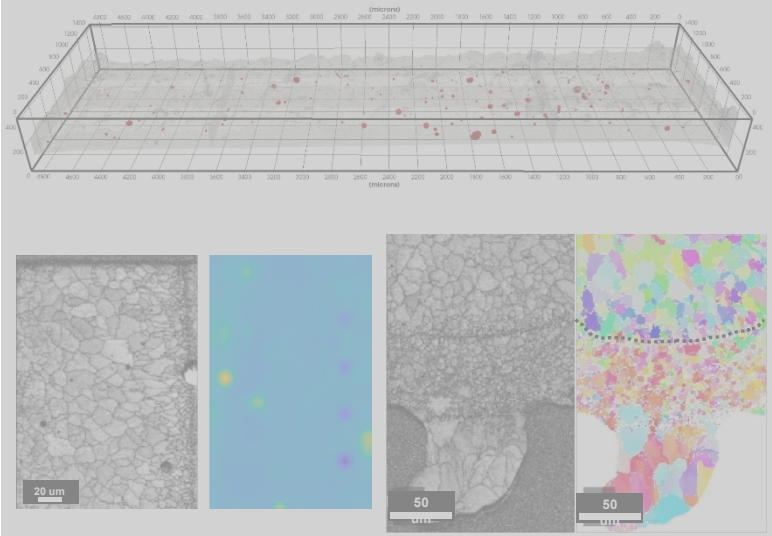

- Identify microstructural features that impact local response (e.g. grain structure and porosity)
- Electron microscopy, micro-computed tomography, nano-indentation

Mechanical Testing

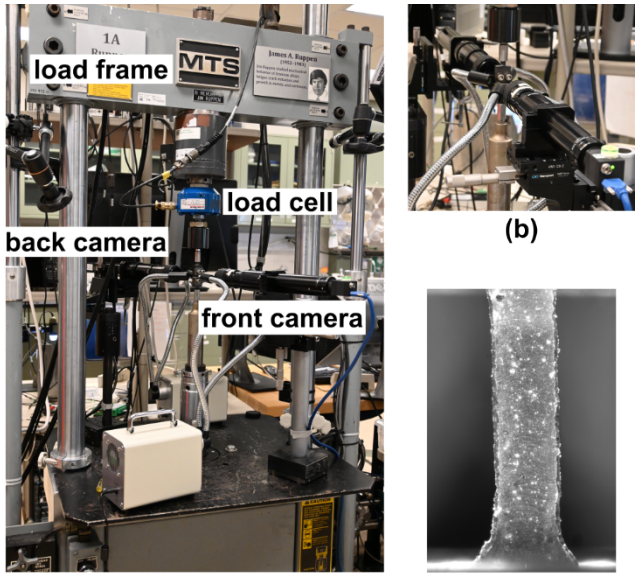

- Determine strength/ductility discrepancies between the surface and interior
- In-situ DIC and micro-computed tomography tensile testing

High-fidelity modeling

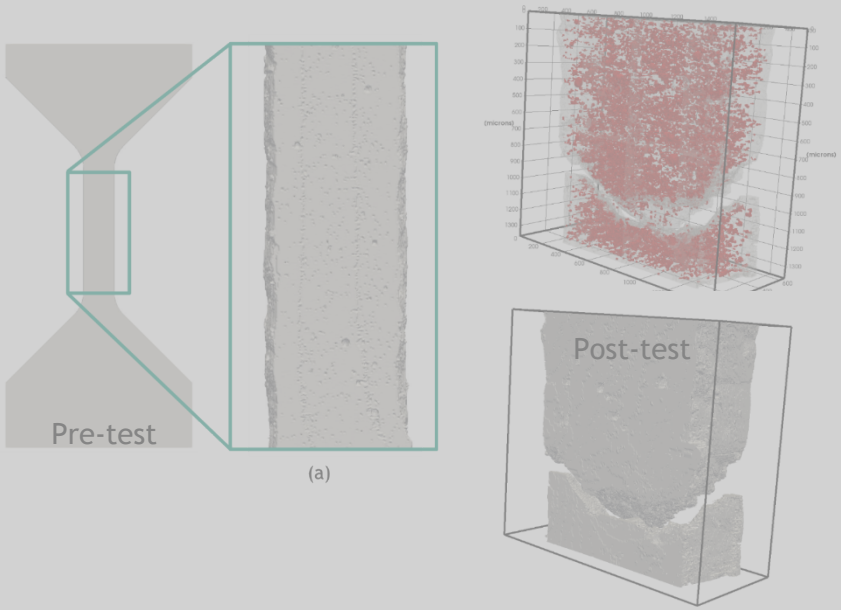

- Determine strength/ductility differences between the surface and interior
- In-situ DIC and micro-computed tomography

Experimental Methods

How do we isolate the edge region for mechanical testing?

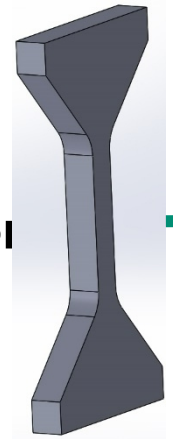

1 mm tensile dogbone

Thin down fabricated samples to leave mostly edge material

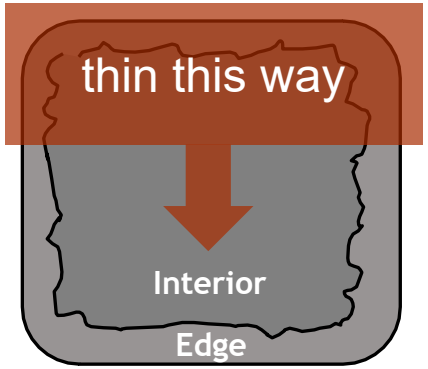

Experimental Methods

How do we isolate the edge region for mechanical testing?

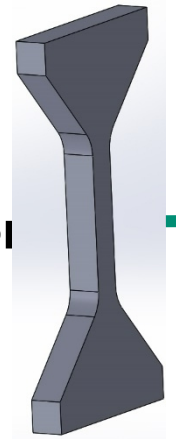

Thin down fabricated samples to leave mostly edge material

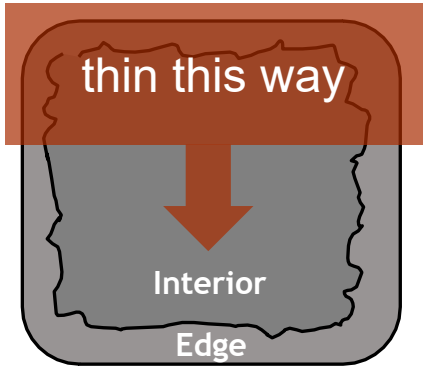

1 mm tensile dogbone

One-sided Thinning

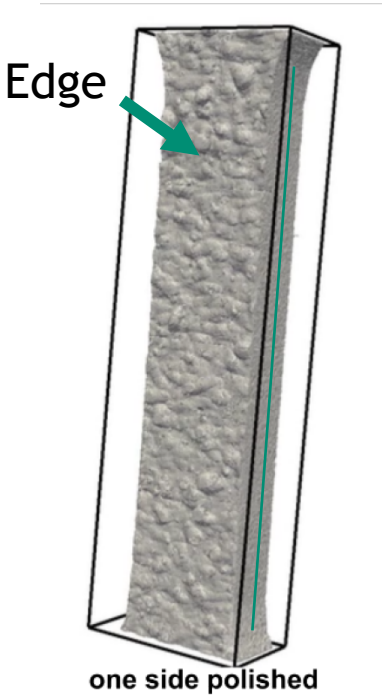

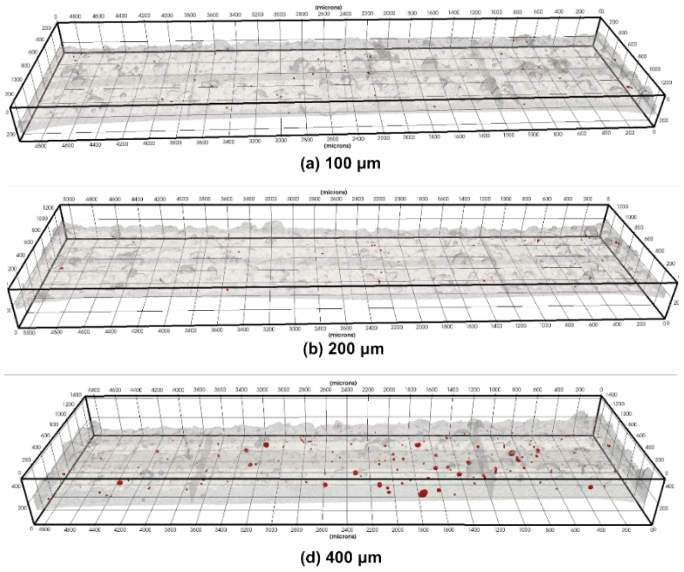

- different thicknesses to vary edge/interior ratio

Two-sided Thinning

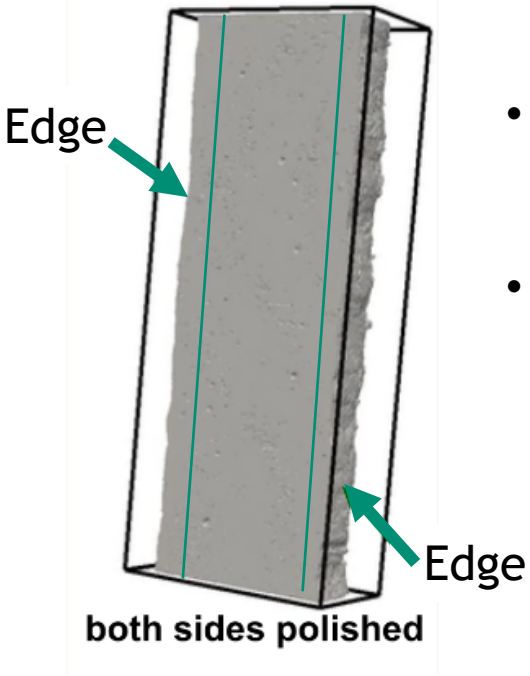

- Thinned to ~500 µm thick
- Edge only on sides of dogbone; allows in-situ observation of failure pogression

Mechanical response of the material from Vendor 1

Sub-sized tensile dogbones

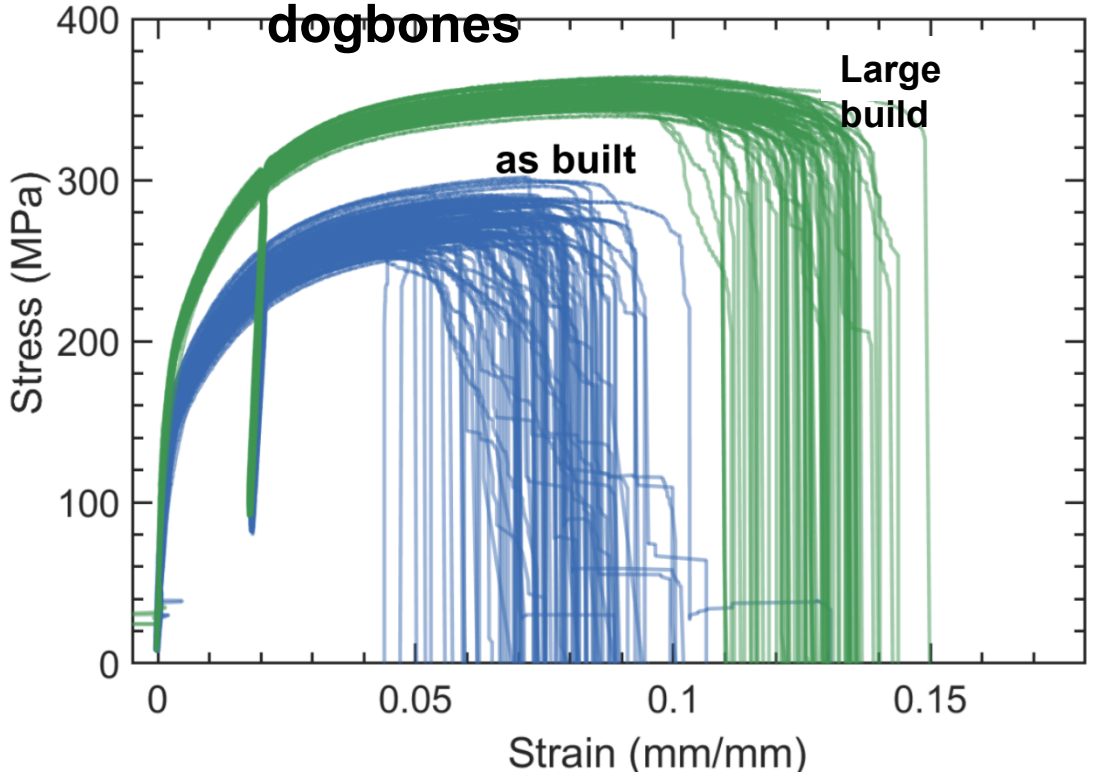

One-sided thinning

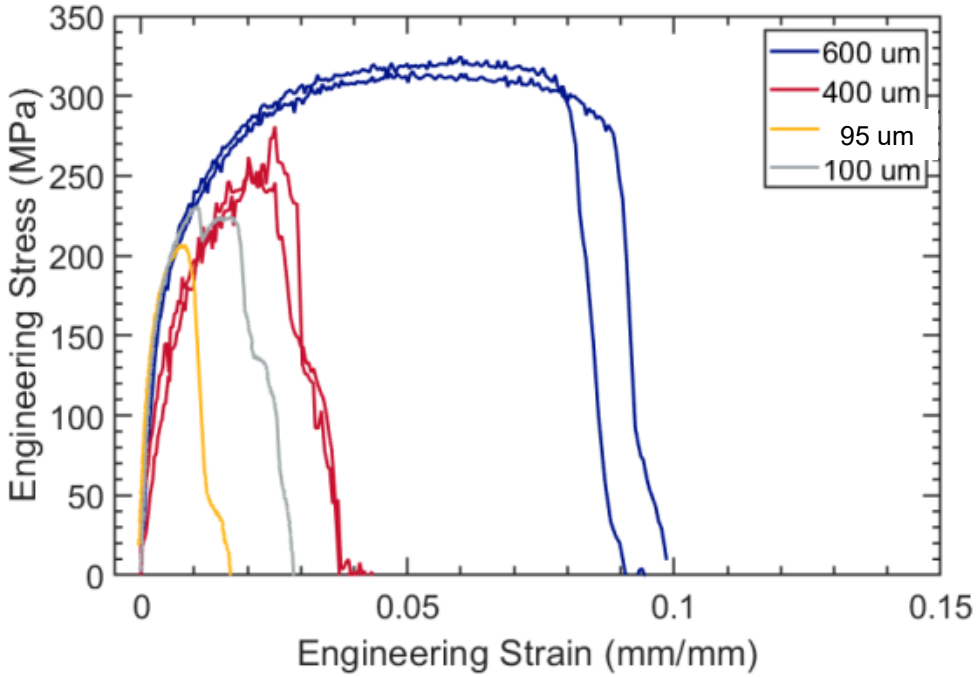

- As-built sub-sized specimens lower strength than those machined from the large block.
- One-sided thinned specimens of 600 um thickness similar to machined response; common elastic response across all the specimens
- Thinner specimens have a reduced capacity for plastic loading; reduced performance is likely attributed to surface defects and texture variation in the edge material increasing damage

Mechanical Response – Vendor 1

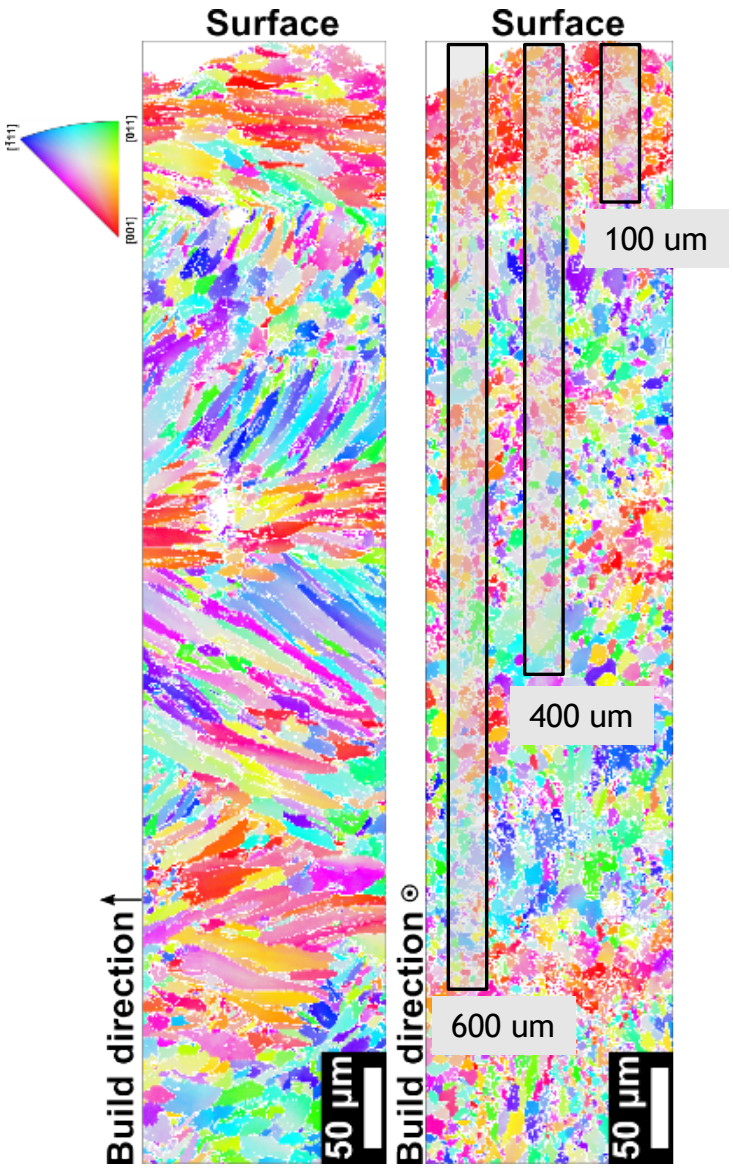

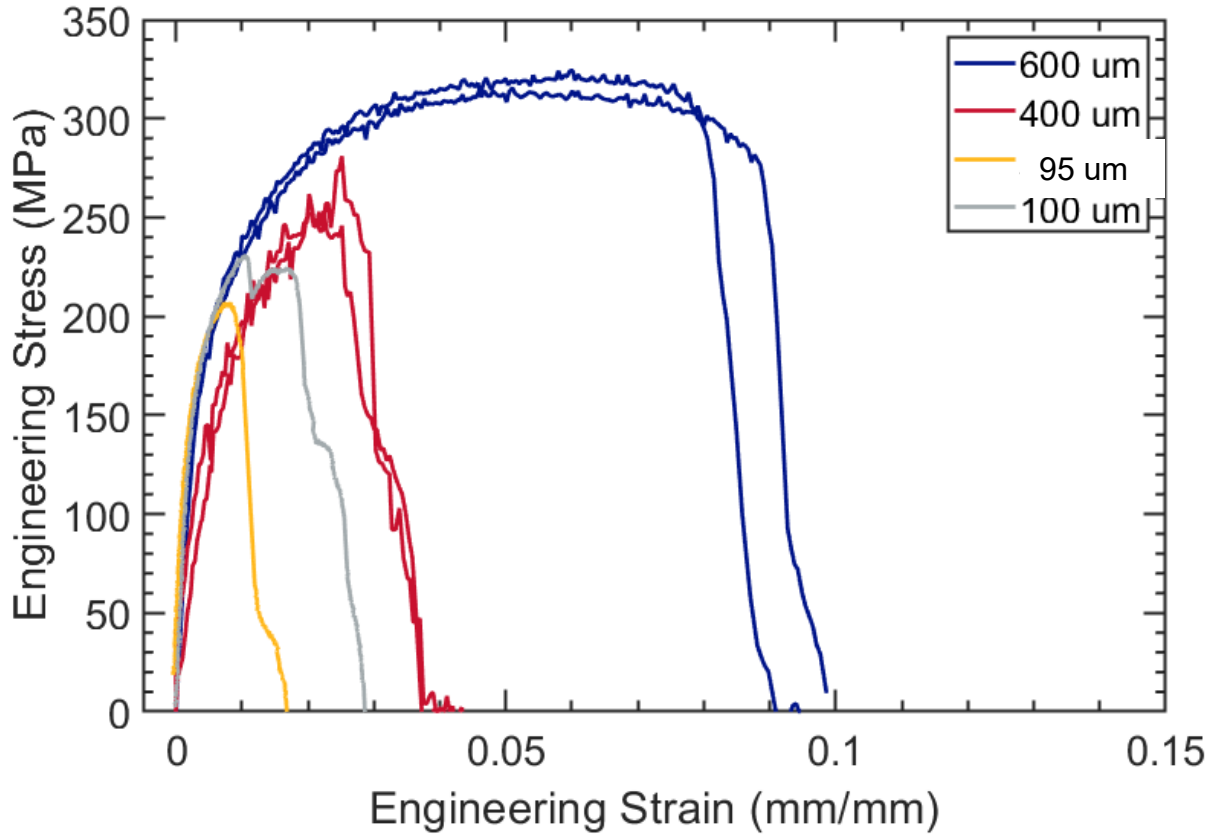

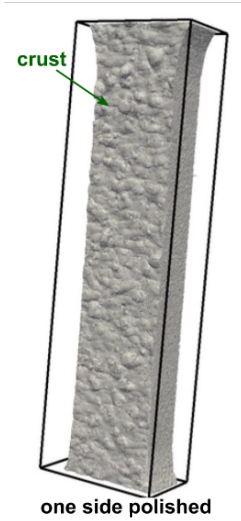

- 100 um thick specimens isolating just the exterior region; little to no contribution from the bulk material
- Defects and poor solidification along the edge likely cause of limited plasticity as damage accumulates rapidly

Experimental Methods

Characterization

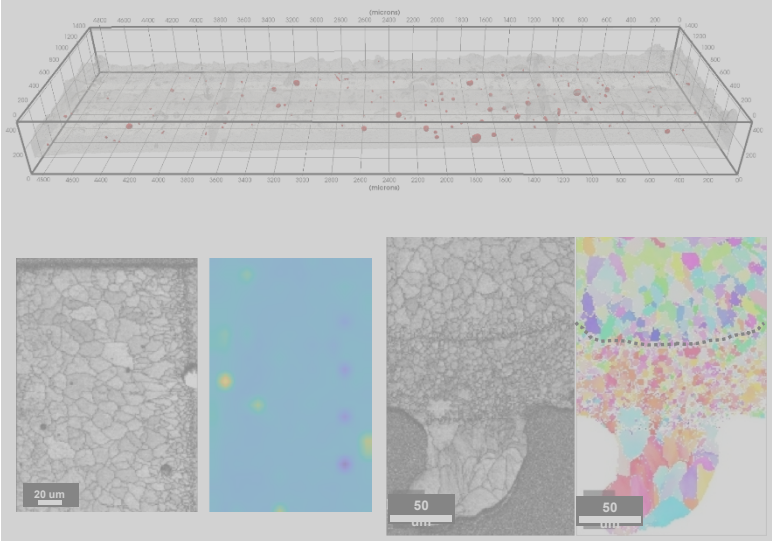

- Identify microstructural features that impact local response (e.g. grain structure and porosity)
- Electron microscopy, micro-computed tomography, nano-indentation

Mechanical Testing

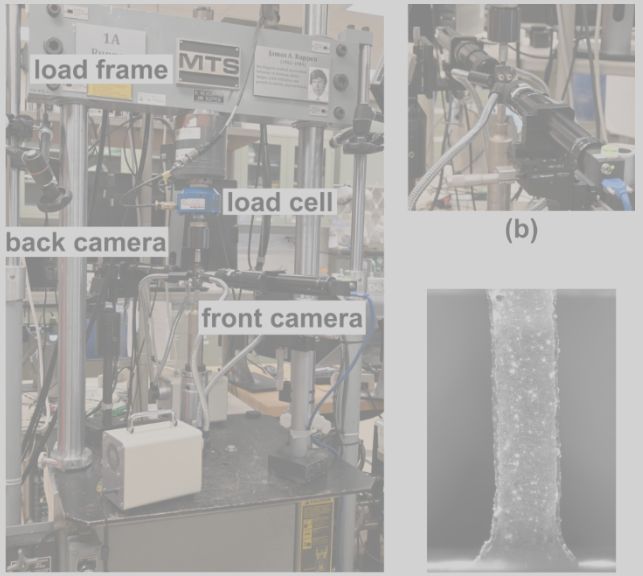

- Determine strength/ductility discrepancies between the surface and interior
- In-situ DIC and micro-computed tomography tensile testing

High-fidelity modeling

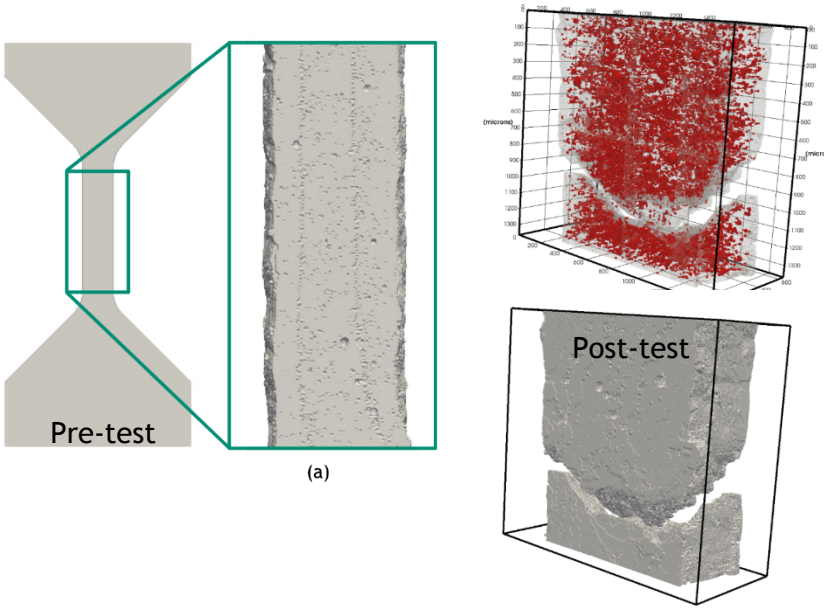

- Determine strength/ductility differences between the surface and interior
- In-situ DIC and micro-computed tomography

Modeling completed directly from in-situ micro-CT results using FEA code in SIERRA with plasticity and local damage

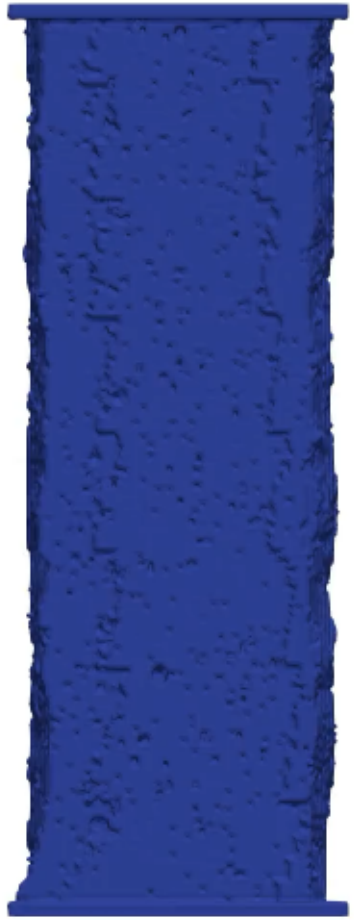

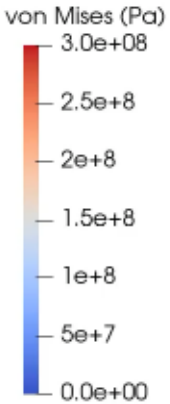

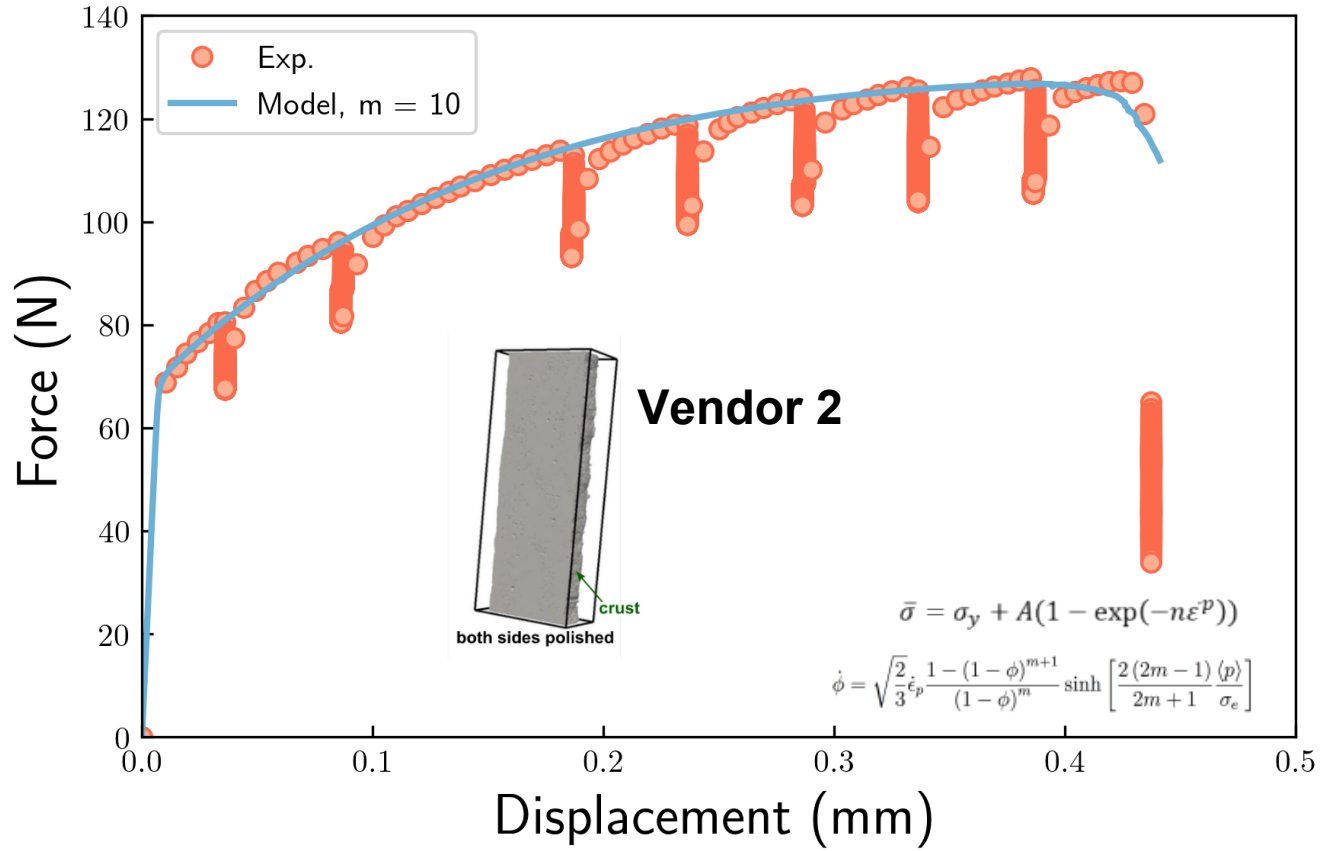

- Predictions for force-displacement follow experimental results after material calibration
- Voce[1] hardening and Cocks-Ashby[2] void growth for damage

[1]Voce, E., J. Inst. Metals 1948
[2]Cocks, A.C.F. and Ashby, M.F., Metal Science

High-fidelity Modeling of In-situ Test

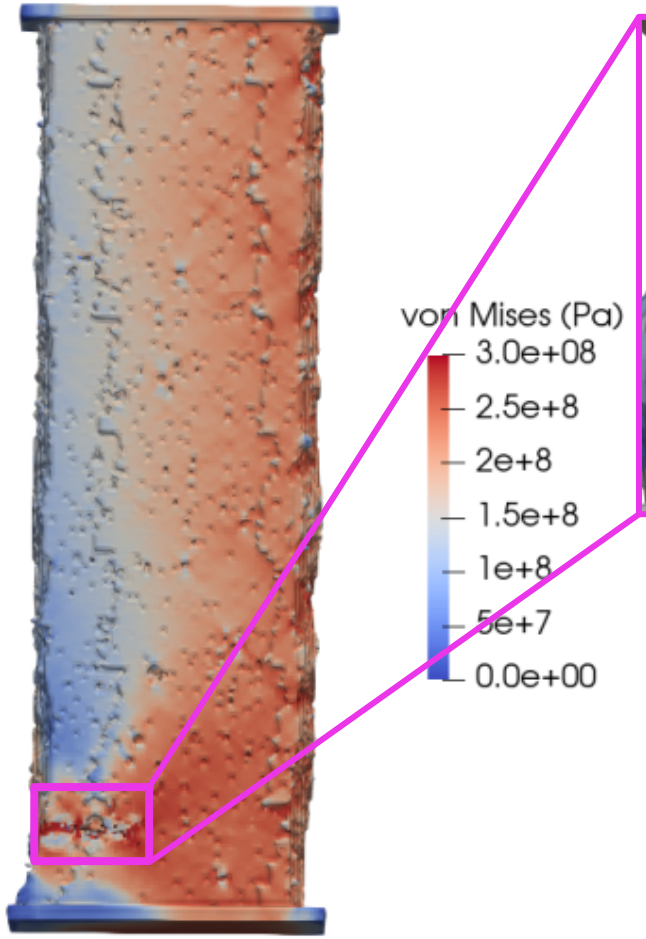

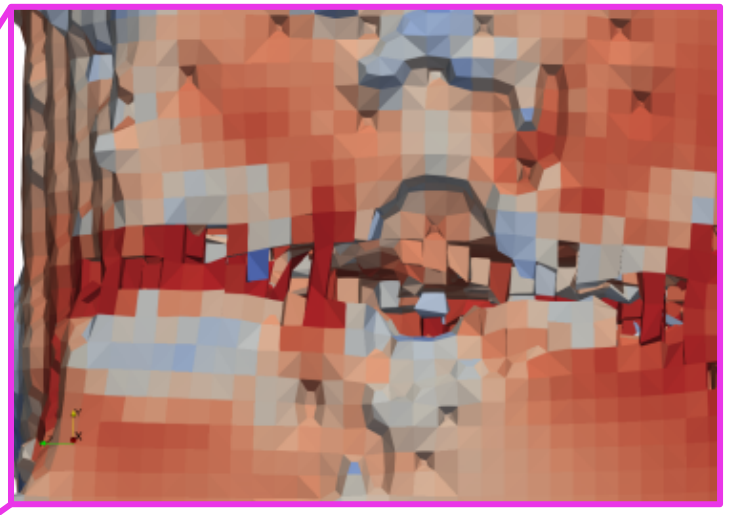

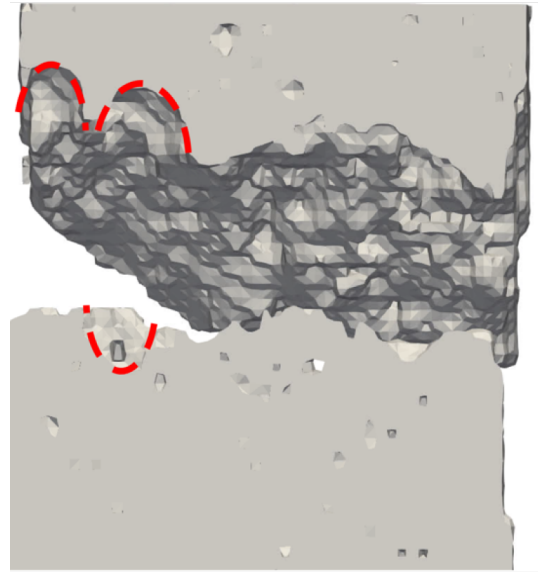

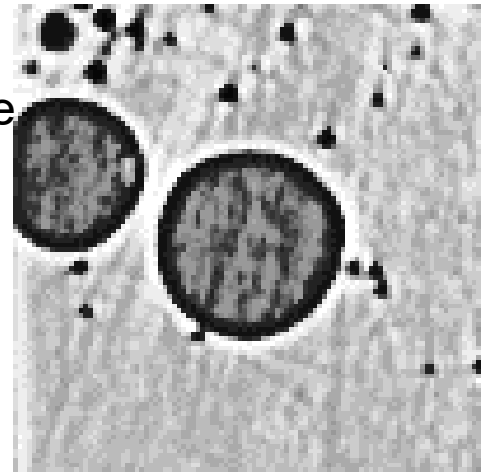

- Failure initiates at two pores near the surface
- Video shows pores growing and merging

- Failure initiation captured during simulation by stress concentration and corresponding damage accumulation

Failure location identified correctly and mechanical response accurately predicted but is dependent on damage parameter selection and mesh resolution

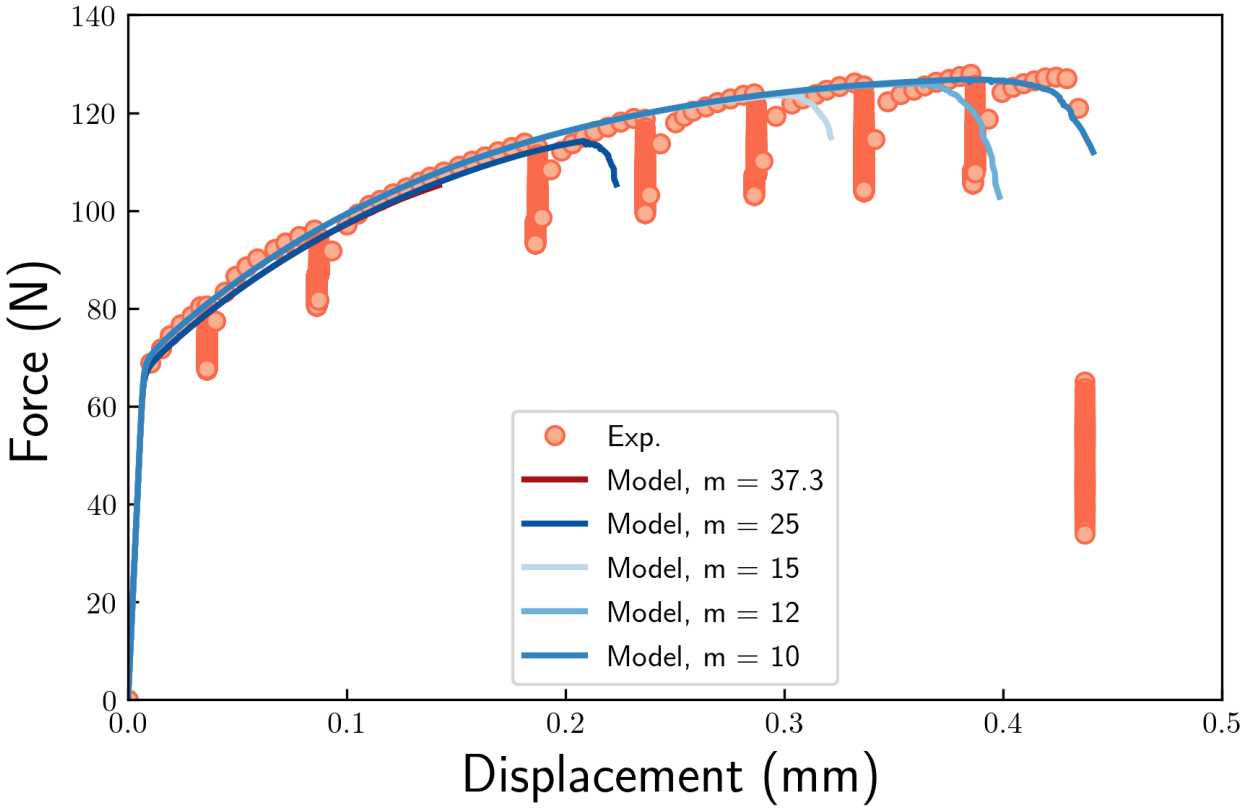

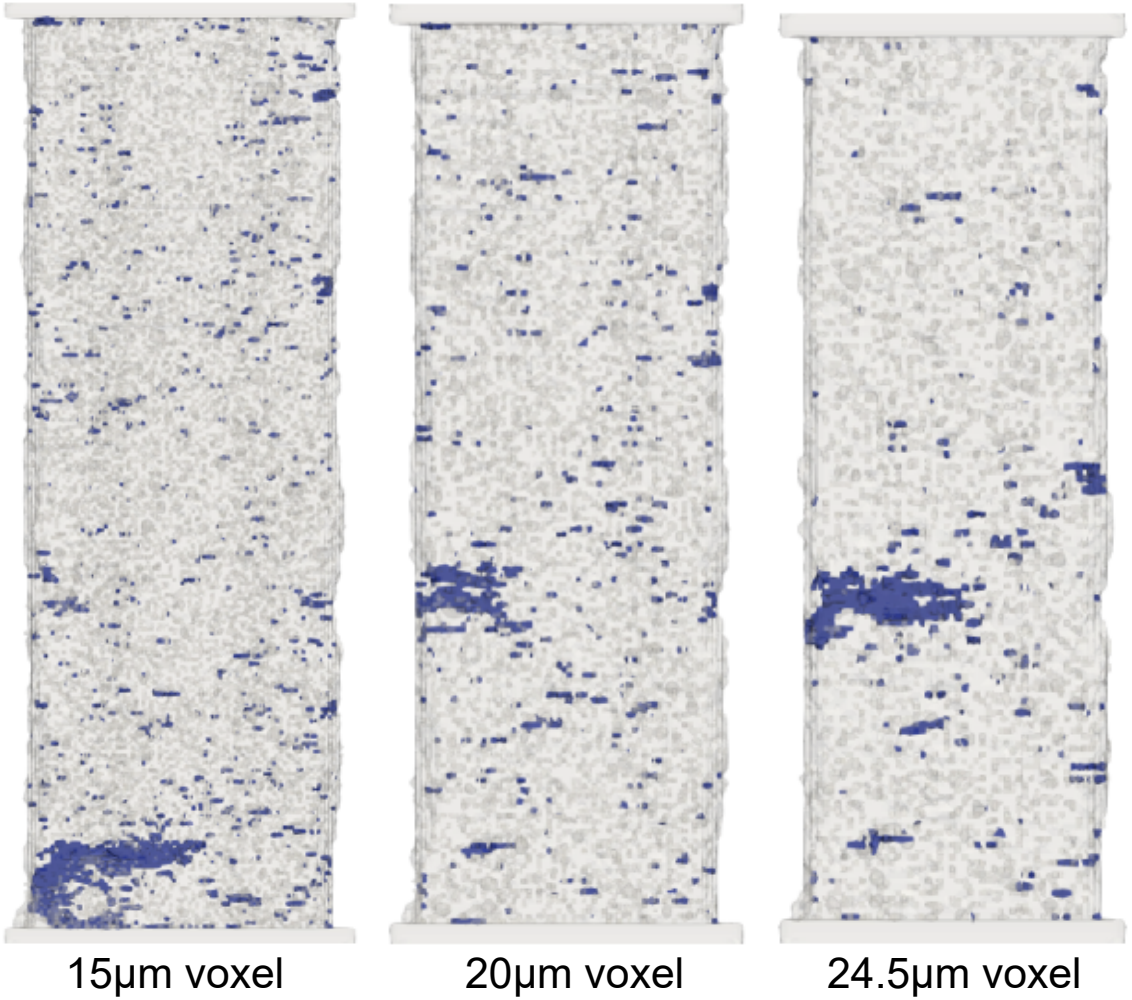

Summary

Key results

- Grain structure along edges contributes to variability in AM
- Local strength gradients not present as a source of variability
- Geometry and surface asperities exert an outsized role in determining failure initiation and progression
- Predicted localized response in AM Al-10Si-Mg using high-fidelity characterizations

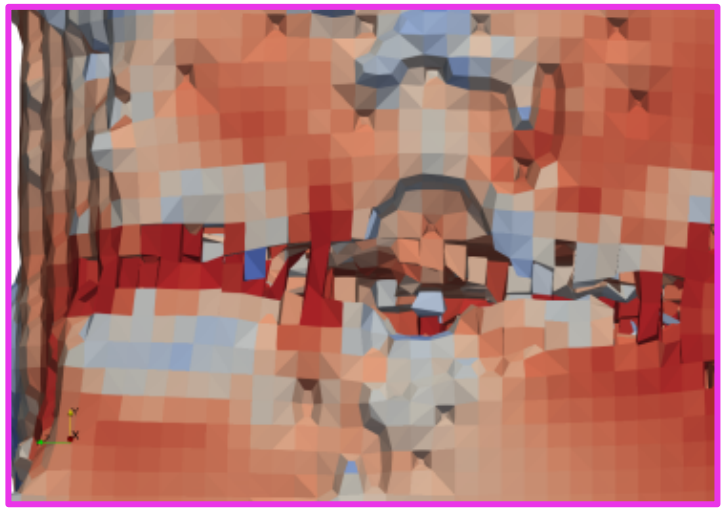

Strain and failure localization along the edge was correctly predicted from high-fidelity modeling

Next steps and challenges

- Perform experiments on complex geometries
- Explore whether these observations are consistent in other alloys
- Does edge behavior have similar impact for fatigue loading?

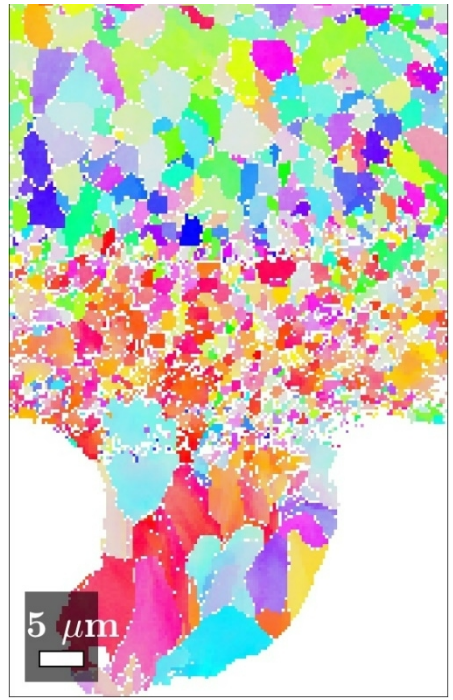

Grain structure variation along the edge of AM Al-10Si-Mg

Backup Slides

Mechanical Response

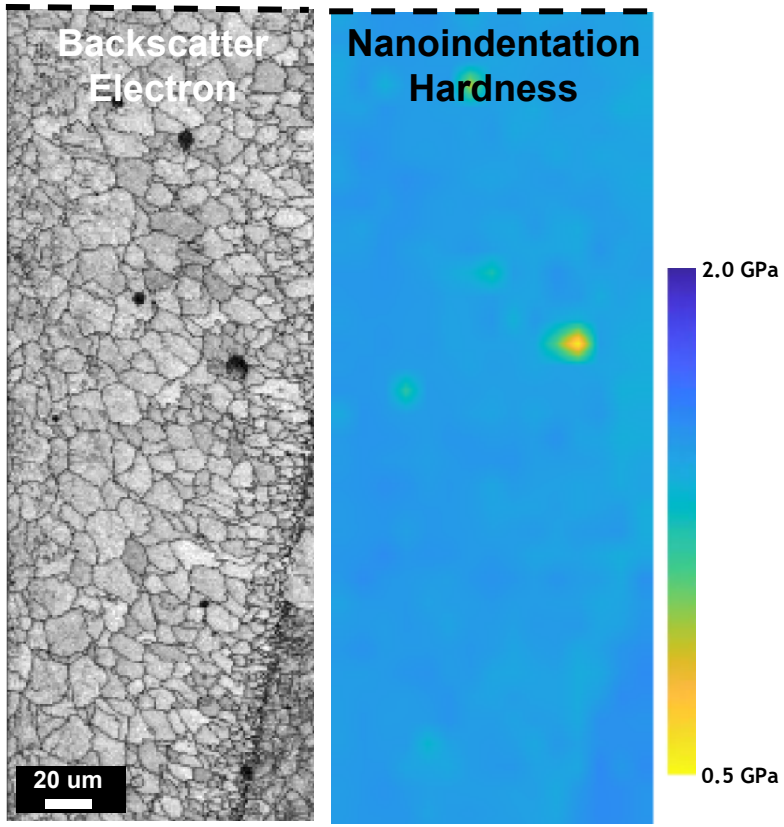

- Nano-indentation did not reveal any gradient in local strength from the edge to the interior of the material

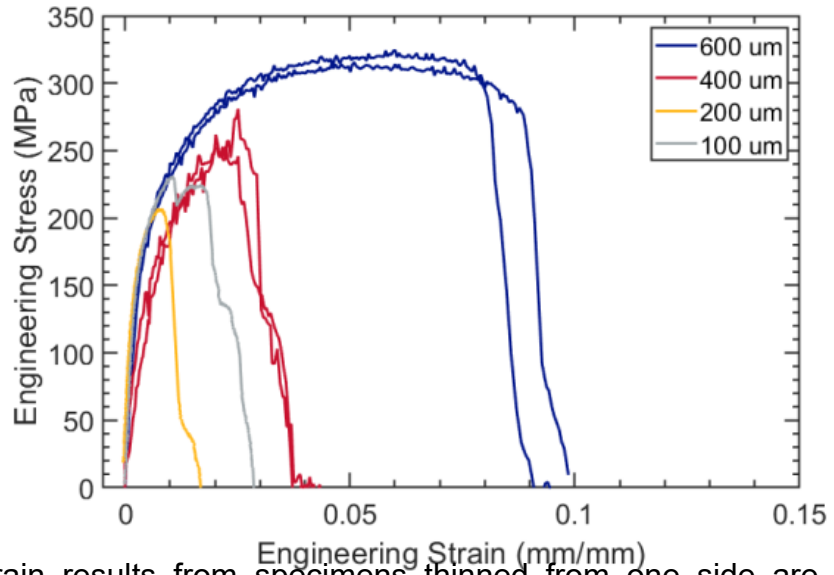

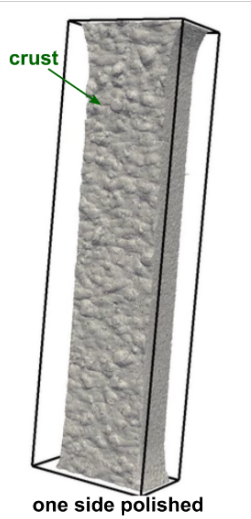

Stress-strain results from specimens thinned from one side are presented in Figure 16. Specimens with thicknesses of 600, 400, 200, and 100 µm are shown on the same plot and distinguished by color. The initial stress-strain behavior is similar between each test but the 400 µm specimens demonstrate slightly different initial slopes, although this may be attributed to test setup variability. As specimen thickness decreases, the strain to failure continually decreases; note that the specimen label 200 µm was actually thinner than the 100 µm specimen by a few microns. These test results demonstrate that ductility decreases significantly with decreasing thickness, which can be attributed to differences in mechanical properties and/or differences in defect content along the crust. Specimens demonstrate a similar stress-strain response with a consistent elastic modulus, but modulus is typically not a strong indicator of mechanical properties since it primarily depends on material chemistry. Additional mechanical properties such as UTS, ductility, and yield strength are stronger functions of thickness. The ACQ material tested has relatively few defects and demonstrates large differences in UTS, ductility, and yield strength. These results suggest that the crust does behave differently than the interior and this effect can be quantified. The precise cause of the reduced performance is likely attributed to surface defects and the texture variation along the crust increasing damage compared to material with the crust removed combined with a decrease in mechanical property values. The nature of how this failure initiates and progresses will be explored using the in-situ testing and specimens polished on both sides.

Mechanical Response

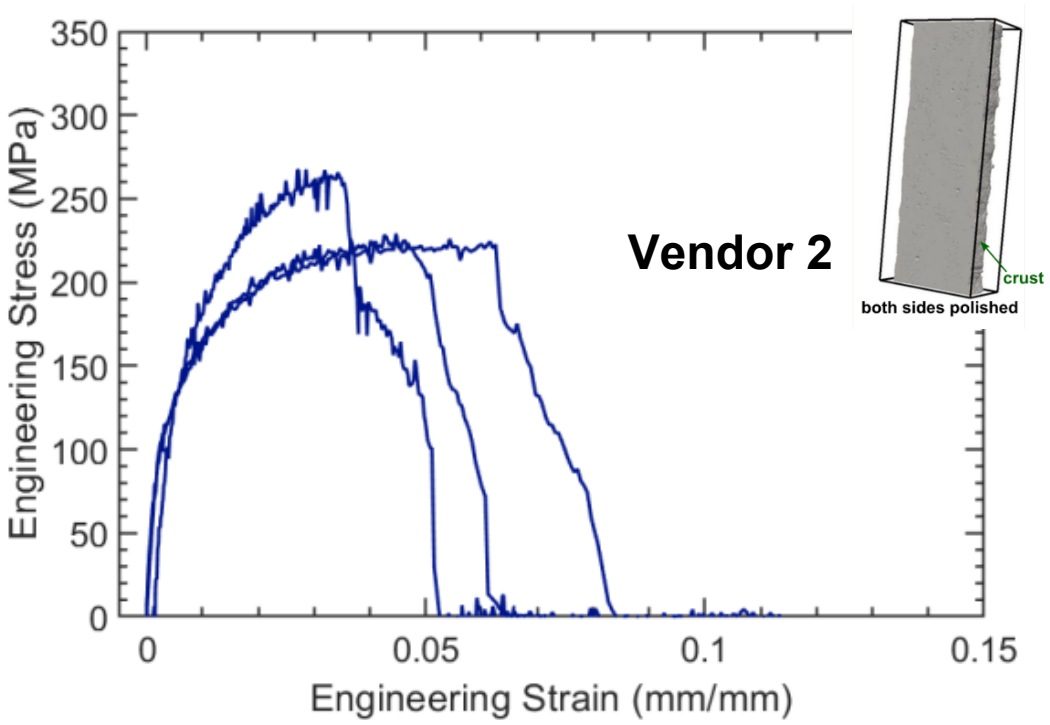

- Stress-strain response similar to the specimens thinned from one side
- Variability between tests from differences in thickness

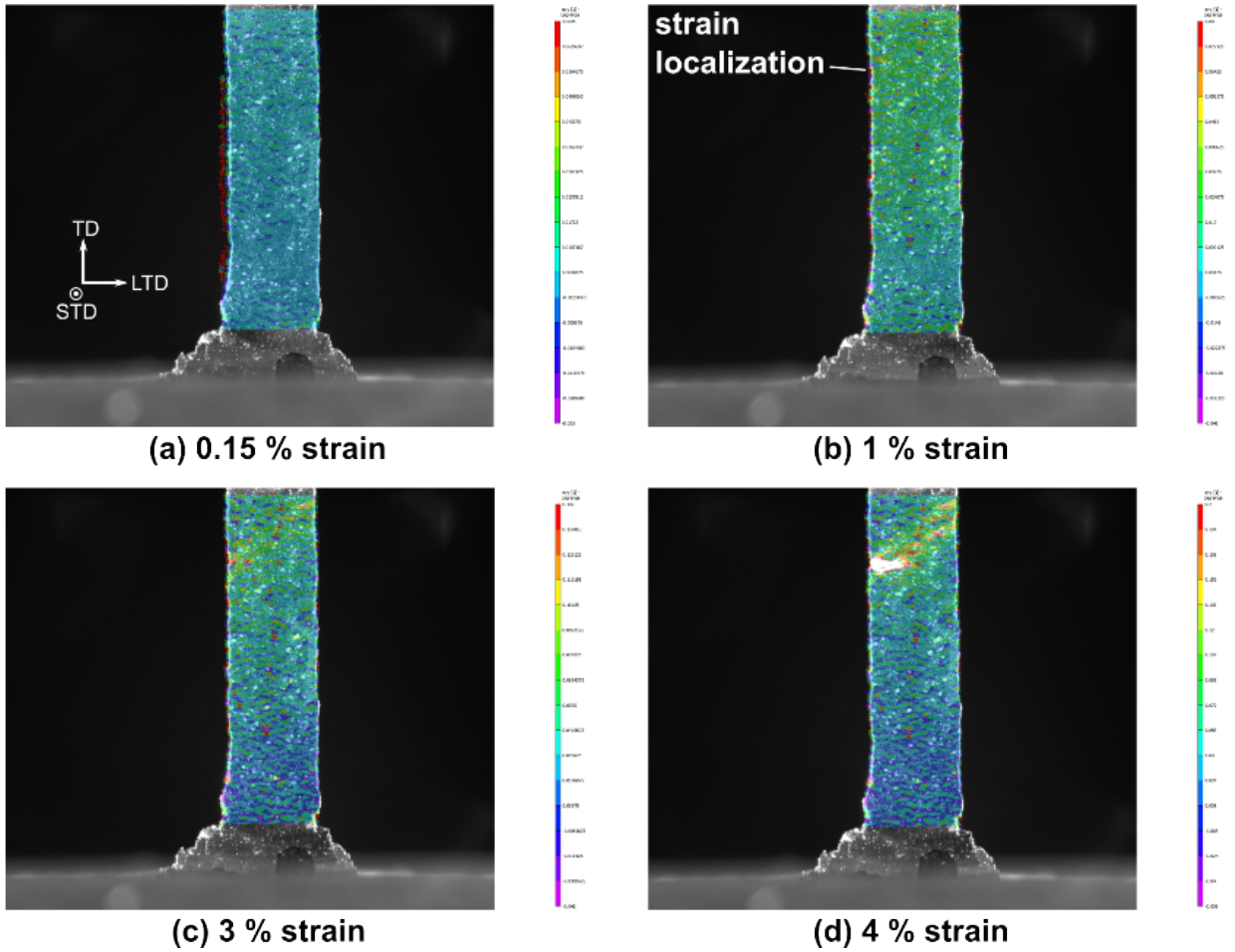

- DIC highlights strain localization along the edge material and formation of a elevated strain band
- Failure spreads from the exterior and across the sample along a path of high strain

Mechanical Response

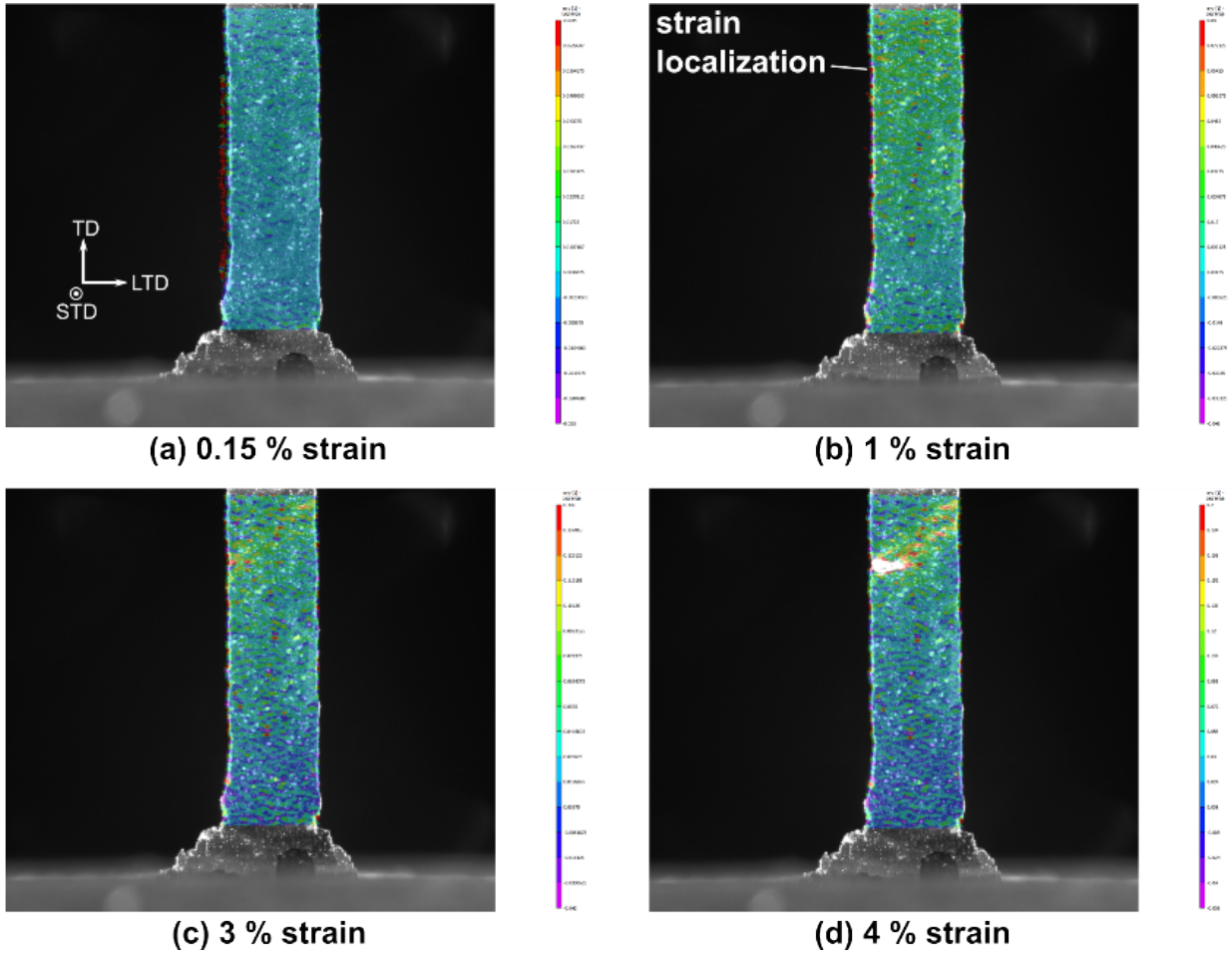

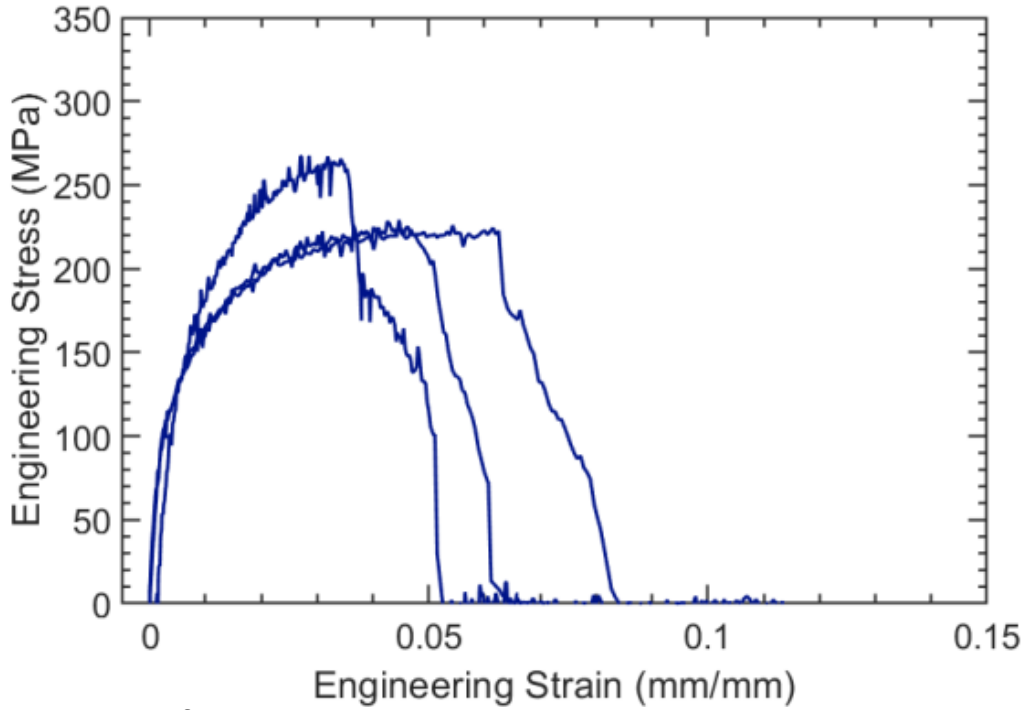

- DIC highlights strain localization along the edge material and formation of a elevated strain band
- Failure spreads from the exterior and across the sample along the strain band

Results from the RATMAM specimens thinned on both sides are presented in Figure 17; specimens were 660, 636, and 438 um thick. The stress-strain response is similar to the ACQ large block specimens thinned from one side to 400 um or less as shown in Figure 16. The variability between tests is likely caused by differences in thickness, with the thicker specimen capable of sustaining more load before initiating failure. The evolution of the strain field as measured from DIC for one of the specimens polished on both sides is provided in Figure 18; strain is shown progressing from 0.15 % strain to 4 % strain, at which point failure initiates. Failure initiates at a strain localization appearing early in the deformation along the exterior edge of the specimen where the crust remained. This localization is the precursor to failure that progresses along a line of high strain that develops at 3 % strain. For all specimens, failure always begins on the short-transverse side of the gage region and follows a high strain line within the specimen. It is suspected that the strain line forms in relation to internal porosity.

Build Parameters

Stress relief anneal both builds:
550 F for 2 hours

Vendor 1

Al	Cu	Fe	Mg	Mn	N	Ni	O	Pb	Si	Sn	Ti
89.57	0.01	0.07	0.3	0.01	0.01	0.01	0.05	0.01	9.78	0.01	0.01

LPBF Tool	SLM 280HL
Hatch Spacing	150 µm
Layer Thickness	30 µm
Laser Power	350 W
Raster Speed	1100 mm/s
Beam Diameter	76.3 µm

Powder size: ASTM B822
20um

Vendor 2

Al	Cu	Fe	Mg	Mn	N	Ni	O	Pb	Si	Sn	Ti
89.57	0.01	0.07	0.3	0.01	0.01	0.01	0.05	0.01	9.78	0.01	0.01

LPBF Tool	EOS M400-1
Hatch Spacing	150 µm
Layer Thickness	60 µm
Laser Power	370 W
Raster Speed	1150 mm/s
Beam Diameter	90 µm

Powder size: ASTM B822
44um – vol% = min 40, max 70
32um - vol% = min 20, max 50
20um - vol% = min 00, max 10

Outline

Motivation and Background

- Jay Carrol's work identified that the surface "crust" in AM Al-10Si-Mg influences mechanical performance
- They saw the crust and determined that it can degrade performance and increase variability, but didn't explore if that region exhibits fundamentally different properties than the interior region.
- Understanding the crust is important because it is unlikely you can always remove it from small or complex parts or if you plan to use AM in an "as-built" state. And if the crust is going to be included in a part, then we need to develop modeling or meshing capabilities that can account for the crust and the variability it may bring to a design.
- The
- We hypothesized that we ca

Project Goals

- Identify regional mechanical behavior in AM metals using microscale, in-situ techniques to inform models
- Determine fracture evolution with in-situ methods and observe deviations around defects and along the transitional region

Material

- Vendor 1 is ACQ material. Describe the build and where specimens were cut from
- Vendor 2 is CarTec material. Describe build and where specimens were cut from.

Microstructure

- Show microstructure of vendor 1 and vendor 2. Note the distinction between the surface and the interior.

Experimental Test Plan

- Base material used as the control

Results

Summary

Model Parameters

Following mesh generation, the mesh underwent simulated tensile loading using the Sierra/SolidMechanics finite element package [5]. The plastic response of the material was captured using Voce isotropic hardening:

$\sigma=\sigma_y+A(1-\exp(-n\varepsilon p))$

where εp is the plastic strain, σ_y is the yield stress, A is the hardening constant, and n is the hardening exponent.

Damage was modeled by accounting for both void nucleation and void growth. Nucleation results in the production of new voids in the material. The void nucleation model takes a form similar to Horstemeyer and Gokhale [6].

$\eta=\eta\varepsilon pN3p\sigma e\#(2)$

where p is the hydrostatic stress, σe is the equivalent stress, $N3$ is the triaxiality constant, and η represents the number of voids per unit volume. Following void nucleation, void growth was modeled by the following equation developed by Cocks and Ashby [7]:

$\phi=23\varepsilon p1-(1-\phi)m+1(1-\phi)m\sinh 2(2m-1)2m+1p\sigma e\#(3)$

where ϕ is damage, and m is the damage exponent. These parameters were analytically calculated to high throughput as-printed tensile data initially, then further calibrated to the in-situ specimen response. The parameter values used in the study can be seen in *Table 5 below.*

Elastic Modulus, E	67.6 GPa
σ_y	138 MPa
A	180 MPa
n	20
m	3.5
N_3	2.0

Model Setup

- Implicit tension models run in Sierra FEA code
- “Pads” added on top and bottom of part to provide force buffer for boundary conditions. *Unnecessary if portion of grips are included in scan
- Cubit/Sculpt creates mesh by converting cartesian grid voxels to hexahedral elements and smoothing edges
- Constitutive response captured with plasticity and local damage models

Voce[1] Hardening

$$\bar{\sigma} = \sigma_y + A(1 - \exp(-n\bar{\varepsilon}^p))$$

Cocks-Ashby[2] Void Growth

$$\dot{\phi} = \sqrt{\frac{2}{3}}\dot{\epsilon}_p \frac{1-(1-\phi)^{m+1}}{(1-\phi)^m} \sinh\left[\frac{2\,(2m-1)}{2m+1}\frac{\langle p\rangle}{\sigma_e}\right]$$

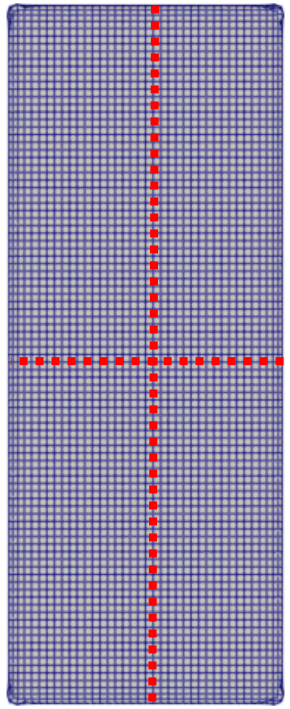

Nodal lateral constraints applied on red lines for Poisson contraction

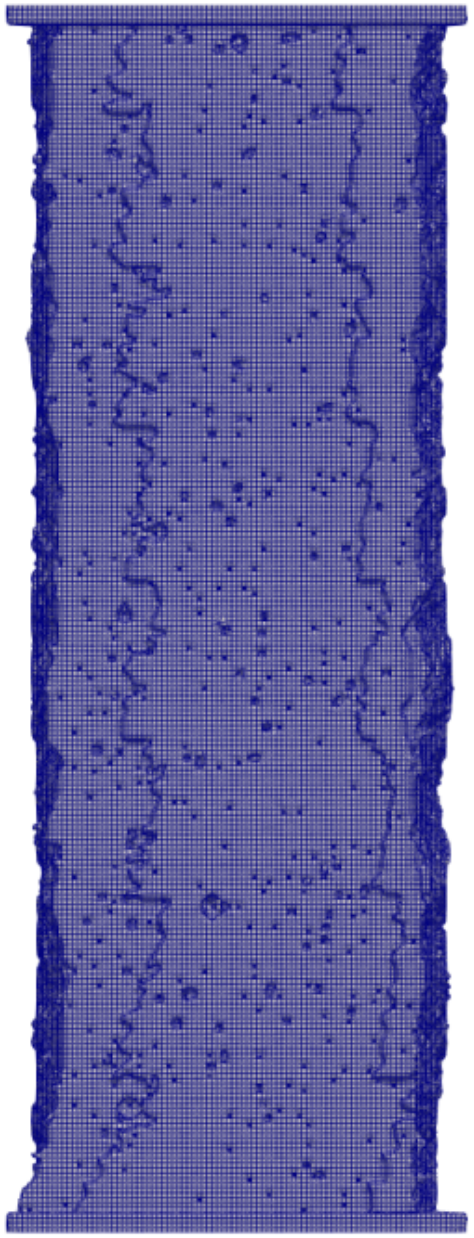

[1]Voce, E., J. Inst. Metals 1948
[2]Cocks, A.C.F. and Ashby, M.F., Metal Science

High-fidelity Modeling

- Material model calibrated using full-size 1 mm dogbones
- Voce isotropic hardening
- Damage from void nucleation and growth
  - Based on Horstemeyer & Gokhale and Cocks & Ashby

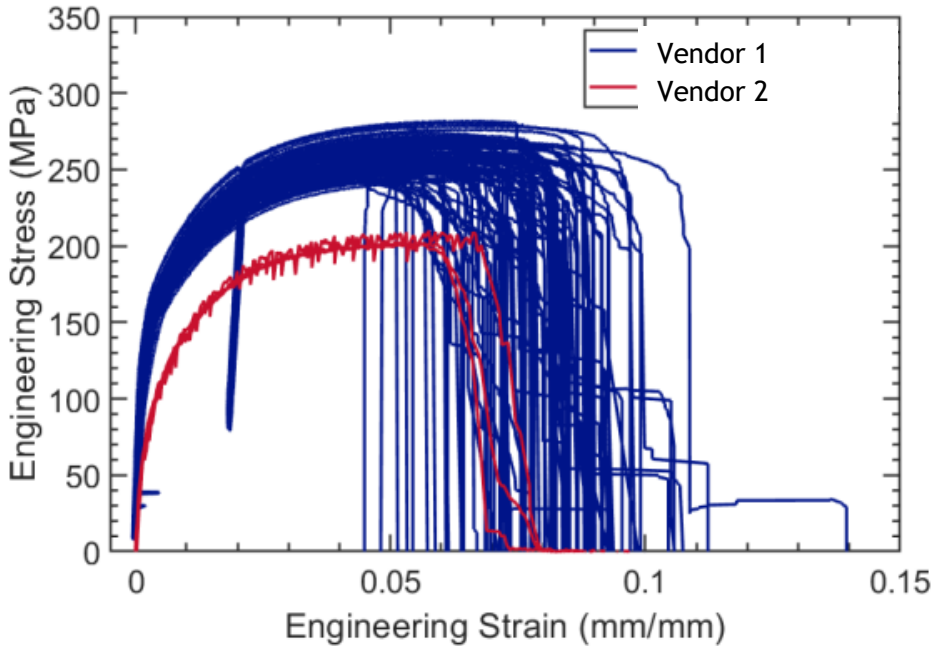

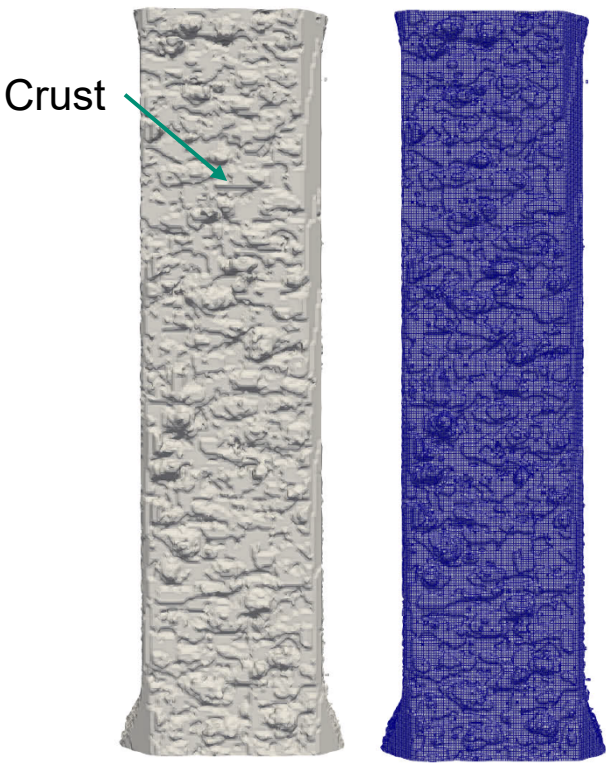

Mesh of tensile specimen CT scan

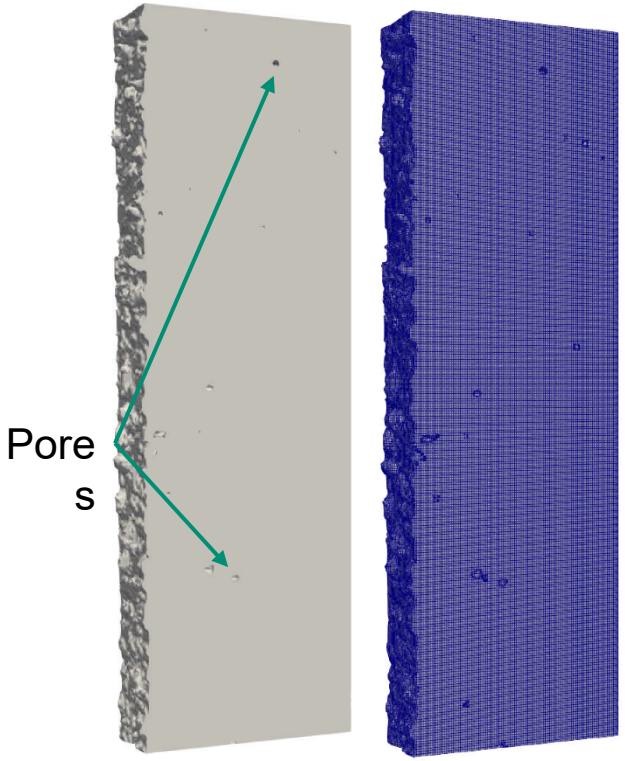

Cut view through center axis

- CT scan directly used to mesh geometry
- Direct numerical simulations (DNS) of these meshes paired with in situ tensile testing allows for comparison of edge, geometry, and pore effects